Differential geometry-based thermodynamics derivation of isotropic and anisotropic eikonal non-local gradient damage models using a micromorphic media framework

Breno RIBEIRO NOGUEIRA, Giuseppe Rastiello, Cédric Giry, Fabrice Gatuingt, Carlo Callari

Differential geometry-based thermodynamics derivation of isotropic and anisotropic eikonal non-local gradient damage models using a micromorphic media framework

Breno Ribeiro Nogueira[a,b], Giuseppe Rastiello[c], Cédric Giry[a], Fabrice Gatuingt[a], Carlo Callari[b]

[a] *Université Paris-Saclay, CentraleSupelec, ENS Paris-Saclay, CNRS, LMPS - Laboratoire de Mécanique Paris-Saclay, 4 avenue des sciences, Gif-sur-Yvette, 91190, , France*

[b] *Università degli Studi del Molise, DiBT, Via Francesco De Sanctis, 1, Campobasso, 86100, , Italy*

[c] *Université Paris-Saclay, CEA, Service d'etudes mécaniques et thérmiques, , Gif-sur-Yvette, 91191, , France*

Abstract

The Eikonal non-local damage (ENL) approach models damage as a space-deforming phenomenon that affects the interaction distance between material points. As damage increases, interactions between points decrease, ultimately resulting in no interaction. In the integral version of such an approach, non-local interaction distances between material points are computed by solving a stationary Hamilton-Jacobi equation with a damage-dependent Riemannian metric. In the implicit gradient version of ENL models, the Riemannian metric figures in the Helmholtz equation to be solved for computing the non-local field controlling damage evolution. However, one of the main criticisms of such formulation is the lack of thermodynamics basis in its derivation. This paper presents a thermodynamics derivation of the Eikonal implicit gradient formulation based on differential geometry concepts to overcome this issue. A free-energy potential is defined considering the non-local strain as a morphological descriptor belonging to the abstract differentiable manifold (where the Riemannian metric is defined). Following a micromorphic media framework, the balance equations of the model are obtained. It is shown that the stress tensor and thermodynamic force associated with damage are the sum of standard and additional non-local contributions. It is also shown that the resulting energy dissipation is always positive, thus verifying the Clausium-Duhem inequality. After presenting all development considering second-order anisotropic continuum damage, the isotropic formulation is obtained as a particular case. Finally, a two-dimensional numerical implementation of an isotropic implicit Eikonal non-local gradient damage model is illustrated. Test cases are simulated to show the relocalization features of the considered formulation and its natural capability of naturally representing damage-to-fracture transition for high damage levels.

Keywords: Eikonal non-local damage, implicit gradient, anisotropic/isotropic damage, thermodynamics, differential geometry

1. Introduction

Complex constitutive relations are often needed to describe general material behaviors. Accordingly, material laws are commonly defined following phenomenological approaches. From elasticity coupled to isotropic and anisotropic damage, several models derived from thermodynamic principles exist (e.g., (Maire and Chaboche, 1997; Faria et al., 1998; Carol et al., 2001; Richard et al., 2010; Desmorat, 2015; Zafati and Richard, 2019)) and allow modeling complex behaviors characterized by hysteresis, crack sliding and friction, unilateral effects, induced anisotropy, etc.

Local damage models fail to predict the fracture process in strain-softening materials, providing physically meaningless results. As already well-known, the boundary value problem becomes ill-posed when localization occurs, and the unicity of the solution cannot be guaranteed (Hadamard, 1903; Thomas, 1961; Hill, 1962; Mandel, 1966; Rudnicki and Rice, 1975; Benallal et al., 1989; Borré and Maier, 1989; Masseron et al., 2022). This is translated into a mesh dependency of the obtained structural response in a numerical finite element context. Non-local theories allow palliating this effect by supposing that the state of a material point inside the domain is influenced by what happens in in the rest of the domain.

Several enriched continuum approaches exist. One can refer, for instance, to Cosserat-type models (Cosserat and Cosserat, 1909), micropolar and micromorphic theories (Eringen and Suhubi, 1964; Mindlin, 1964; Suhubl and Eringen, 1964; Eringen and Kafadar, 1976; Eringen, 1999), and gradient theories (Aifantis, 1984; Frémond and Nedjar, 1996; Lorentz and Andrieux, 1999). Other approaches are more numerically oriented and mainly aim at introducing a characteristic length scale (l_c) into the formulation to avoid the ill-posedness of the problem without establishing direct links with microstructural phenomena. In this latter case, non-locality can be mainly considered as mathematical tool (a localization limiter) to regularize the response provided by the model. Among them, it is worth citing integral non-local formulations (Pijaudier-Cabot and Bažant, 1987), implicit gradient formulations (Peerlings et al., 1996, 2004), the thick level-set model (Moës et al., 2011), phase-field formulations (Francfort and Marigo, 1998; Bourdin et al., 2000; Miehe et al., 2010; Pham et al., 2011), and more recently the "Lip-field" approach to damage (Moës and Chevaugeon, 2021; Chevaugeon and Moës, 2022).

Integral and implicit gradient non-local formulations, in particular, are often used for treating continuum damage mechanics problems. A main drawback of the standard non-local regularization methods consists, however, in nonphysical interactions of material points across damaged bands and holes or close to free boundaries (Geers et al., 1998; Simone et al., 2004; Krayani et al., 2009). Different formulations have been proposed in the literature to reduce such parasite effects. In particular, non-local interactions evolving with mechanical fields (e.g., stress, strain, damage) were introduced by different authors (Geers et al., 1998; Pijaudier-Cabot et al., 2004; Simone et al., 2003; Nguyen, 2011; Giry et al., 2011; Saroukhani et al., 2013;

Desmorat and Gatuingt, 2007; Desmorat et al., 2015) to better model strain localization, thus indirectly describing a progressive damage-to-fracture transition.

The ENL formulation (Desmorat et al., 2015) provides a geometrical interpretation of damage dependent evolving non-local interactions, both in isotropic and anisotropic contexts. From a differential geometry viewpoint, this approach states that damage induces a curvature of the Riemannian space in which interaction distances are computed (figure 1). From a mathematical point of view, interaction distances between material points are computed as solution of an isotropic time-independent Eikonal equation with a damage dependent metric function. In a integral non-local framework, geodesic interaction distances computed in the curved space are thus used to obtain non-local variables driving the damage evolution (Rastiello et al., 2018; Jirásek and Desmorat, 2019; Thierry et al., 2020), thus preserving the general theoretical framework of integral non-local theories. An equivalent implicit gradient ENL formulation (called ENLG in the remainder of this manuscript) was also developed by Desmorat et al. (2015), following the same procedure used by Peerlings et al. (1996) to derive the standard implicit gradient (GNL) formulation from the integral non-local formulation by Pijaudier-Cabot and Bažant (1987). The resulting formulation is very close to the original GNL model, with the main difference that the damage dependent metric now intervenes directly in the Helmholtz differential equation that needs to be solved to compute the field (e.g., an equivalent non-local strain field) controlling damage evolution. A non-intrusive implementation of this approach applied to a damage-plastic model can be found in (Marconi, 2022).

One of the main criticisms of these regularization techniques is that they lack a well-defined thermodynamic background. In these models, the variable controlling damage growth is usually taken as the non-local equivalent strain, whereas the damage variable remains purely local. Thus, the intrinsic energy dissipation is evaluated following the standard thermodynamics theory (i.e., no effects of non-locality are taken into account in the free-energy potential).

To overcome this issue, Peerlings et al. (2004) proposed a thermodynamics framework for deriving the GNL model. The non-local equivalent strain and its gradient were considered state variables in the free-energy potential, together with damage and the displacement field. To account for non-local interactions and the exchange of energy in the entire body, the Clausius-Duhem inequality was globally verified (i.e., the positivity of the total dissipation on the whole body was exploited). Constitutive relations were derived following usual arguments, leading to a modification of the elasticity law. The Helmholtz differential equation was derived with no need to define some generalized stresses. A very similar free-energy potential was proposed in (Forest, 2009), where the micromorphic approach was used to derive the same equations of the model, with the explicit contribution of generalized terms in the local energy balance. Other equivalent techniques introduce a residual term, respecting an insulation condition, in the point-wise Clausius-Duhem inequality, taking into account the energy exchange between neighbor points (Polizzotto et al., 1998; Borino

et al., 1999; Polizzotto, 2003).

The present work provides a thermodynamic derivation of the ENLG model based on the micromorphic media framework. A first form of the free energy potential is proposed, entirely based on the one introduced for the GNL model in Peerlings et al. (2004). The equations of the ENLG model are first obtained following the approach proposed by (Forest, 2009). It is shown that the using standard approaches leads to some thermodynamic inconsistencies related to intrinsic energy dissipation and Cauchy stress tensor definitions.

Such inconsistencies are eliminated when a geometric description consistent with the initial assumption of ENL models is used. A second form of the free energy potential is then proposed. In this case, the non-local strain is considered a morphological description of the abstract differentiable manifold where the Riemannian metric is defined (i.e., it is defined on a Riemannian space deformed by damage). Employing differential geometry concepts, all the equations of the ENLG non-local model can then be derived. It is also shown that the expression of the energy dissipation for the ENLG model differs from the usual ones considered in the classic non-local models.

The paper is structured as follows. The formulations of the GNL and ENLG damage models are briefly recalled first, and the boundary value problem is defined in its weak (variational) form. A free-energy potential is then proposed and isotropic and anisotropic derivations of the ENLG model are presented. The second part of the paper addresses a geometric description of the thermodynamics introduced before. A recall on some useful elements of differential geometry is therefore provided. The equations of the ENLG model are obtained again and the expressions of the energy dissipation in anisotropic and isotropic damage are derived. Then, a brief comparison with other formulations is presented. Finally, numerical simulations compare the GNL and ENLG models regarding structural response, damage profiles, and "pseudo-crack" paths.

2. Gradient-enhanced damage models: GNL and ENLG

After illustrating the GNL formulation, this section presents the ENLG model considering a second-order damage tensor ($\mathbf{D}$) for describing material degradation (its principal components (D_i) take values between zero (sound material) to unity (totally damaged material) in the corresponding directions). Then, the variational boundary value problem to be solved is introduced.

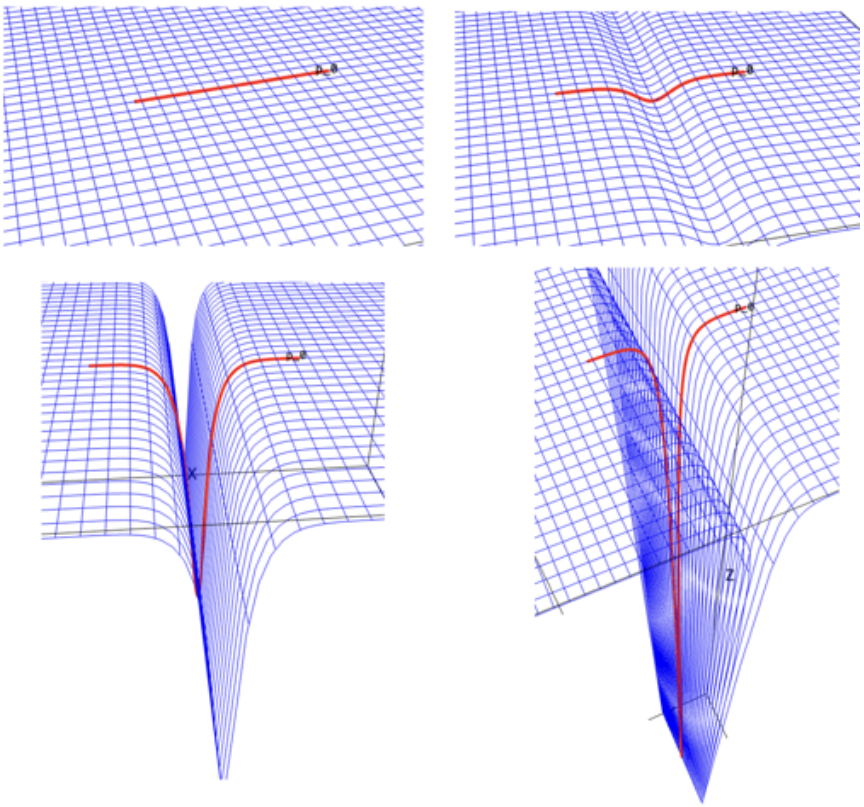

Figure 1: Qualitative representation of damage curving the space where non-local interactions take place. An exponential isotropic damage profile was considered in one direction to compute the metric field. From top left to bottom right, snapshots are given at increasing damage levels in the middle of the damaged band. The red line represents the geodesic path between two points separated by the damaged zone. Computations were carried out with the SageManifolds project, within the open-source SageMath software (The Sage Developers, 2022). Similar results where obtained by Rastiello et al. (2018) using a Fast-Marching method to solve the Hamilton-Jacobi equation controlling damage dependent non-local interaction distances.

2.1. GNL model

According to the GNL model, the differential problem to be solved for computing the non-local equivalent strain field driving damage reads:

$$\bar{e} - c\nabla^2\bar{e} = e \qquad \text{on } \Omega \tag{1}$$

$$\nabla\bar{e} \cdot \boldsymbol{n} = 0 \qquad \text{on } \partial\Omega \tag{2}$$

where "∇^2" is the Laplace operator, "∇" is the gradient operator, symbol "$\cdot$" denotes the simple contraction operator between tensors, Ω is the domain under consideration, $\partial\Omega$ denotes its boundary, $\boldsymbol{n}$ is the outward unity vector to $\partial\Omega$, e is the local equivalent strain, $\bar{e}$ is its nonlocal counterpart, and $c > 0$ is the gradient parameter (homogeneous to the square of a length).

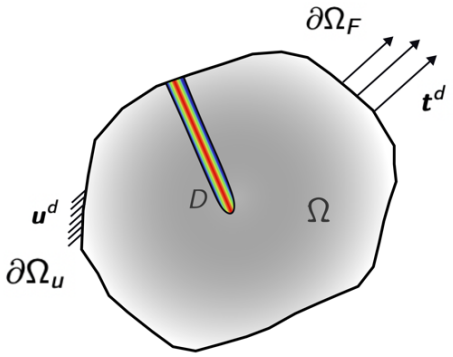

Figure 2: Domain and boundary conditions.

2.2. ENLG model

The ENLG regularization (Desmorat et al., 2015) naturally considers non-local interactions which are function of the damage state (represented through the second-order damage tensor $\mathbf{D}$). This agrees with the desired characteristics described by Bažant et al. (2022) for non-local models to represent the crack-parallel stresses well. The resulting differential problem to be solved can be written as:

$$\bar{e} - c\frac{1}{\sqrt{\det \mathbf{g}}}\nabla \cdot \left(\sqrt{\det \mathbf{g}}\, \mathbf{g}^{-1} \cdot \nabla \bar{e} \right) = e \qquad \text{on } \Omega \tag{3}$$

$$\mathbf{g}^{-1} \cdot \nabla \bar{e} \cdot \boldsymbol{n} = 0 \qquad \text{on } \partial\Omega \tag{4}$$

where "$\nabla\cdot$" denotes the divergence operator. Here, the second order tensor $\mathbf{g}$ is the damage-dependent Riemannian metric:

$$\mathbf{g} = (\mathbf{I} - \mathbf{D})^{-1} \tag{5}$$

with $\mathbf{I}$ being the second-order identity tensor. Notice that according to (3), $\det \mathbf{g} > 0$.

2.3. ENLG boundary value problem (BVP)

Let us consider a n-dimensional solid body $\Omega \subset \mathbb{R}^n$, with $n \in [\![1, 3]\!]$ (figure 2). Neumann conditions are applied on $\partial\Omega_t \subset \mathbb{R}^n$ and Dirichlet conditions on $\partial\Omega_u \subset \mathbb{R}^n$, such as $\partial\Omega = \overline{\partial\Omega_t \cup \partial\Omega_u}$ and $\partial\Omega_t \cap \partial\Omega_u = \emptyset$. Quasi-static conditions are considered. Given this choice, the time dependence of all quantities is omitted in the following, and all the variables introduced should be referred to the present time $t \in [0, T]$ with T being the total time.

Admissibility spaces. Let us introduce the following functional spaces:

$$\mathcal{U} = \{\boldsymbol{w} \mid \boldsymbol{w} \in H^1(\Omega) \ , \ \boldsymbol{w} = \boldsymbol{u}^d \ \text{on}\, \partial\Omega_u\} \tag{6}$$

$$\mathcal{U}(\mathbf{0}) = \{\boldsymbol{w} \mid \boldsymbol{w} \in H^1(\Omega) \ , \ \boldsymbol{w} = \mathbf{0} \ \text{on}\, \partial\Omega_u\} \tag{7}$$

$$\mathcal{V} = \{w \mid w \in H^1(\Omega)\} \tag{8}$$

where $\boldsymbol{u}^d = \boldsymbol{u}^d(\boldsymbol{x}) : \partial\Omega_u \to \mathbb{R}^n$ is the imposed displacement on $\partial\Omega_u$ and H^1 denotes a square integrable Sobolev space.

Equilibrium problem. Neglecting body forces, and under quasi-static conditions, the variational equilibrium problem to be solved consists in finding at each time t, the admissible displacement field $\boldsymbol{u} \in \mathcal{U}$ satisfying:

$$\int_\Omega \boldsymbol{\sigma}(\boldsymbol{\epsilon}(\boldsymbol{u}), \mathbf{D}) : \boldsymbol{\epsilon}(\boldsymbol{v})\, dV = \int_{\partial\Omega_t} \boldsymbol{t}^d \cdot \boldsymbol{v}\, dS \ \ \forall\, \boldsymbol{v} \in \mathcal{U}(\mathbf{0}). \tag{9}$$

where $\boldsymbol{u} = \boldsymbol{u}(\boldsymbol{x}) : \Omega \to \mathbb{R}^n$ is the displacement vector field, $\boldsymbol{v} = \boldsymbol{v}(\boldsymbol{x}) : \Omega \to \mathbb{R}^n$ is a virtual displacement field, $\boldsymbol{\sigma}(\boldsymbol{\epsilon}(\boldsymbol{u}), \mathbf{D})$ is the Cauchy stress tensor, $\boldsymbol{\epsilon}(\boldsymbol{u})$ (respectively, $\boldsymbol{\epsilon}(\boldsymbol{v})$) is the small strain tensor applied to $\boldsymbol{u}$ (respectively, $\boldsymbol{v}$), ":" denotes the double contraction between tensors, and $\boldsymbol{t}^d = \boldsymbol{t}^d(\boldsymbol{x}) : \partial\Omega_t \to \mathbb{R}^n$ is the imposed traction vector on $\partial\Omega_t$.

Damage problem. The variational form of the Helmhotz equation (3) reads:

$$\int_\Omega \sqrt{\det \mathbf{g}}\, \bar{e}\, \eta dV - \int_\Omega c\nabla \cdot (\sqrt{\det \mathbf{g}}\, \mathbf{g}^{-1} \cdot \nabla \bar{e})\eta dV = \int_\Omega \sqrt{\det \mathbf{g}}\, e\eta dV \quad \forall\, \eta \in \mathcal{V} \tag{10}$$

where $\eta = \eta(\boldsymbol{x}) : \Omega \to \mathbb{R}$ is a virtual non-local equivalent strain field. Using the identity:

$$c\nabla \cdot (\sqrt{\det \mathbf{g}}\, \mathbf{g}^{-1} \cdot \nabla \bar{e}\eta) = c\nabla \cdot (\sqrt{\det \mathbf{g}}\, \mathbf{g}^{-1} \cdot \nabla \bar{e})\eta + c(\sqrt{\det \mathbf{g}}\, \mathbf{g}^{-1} \cdot \nabla \bar{e}) \cdot \nabla \eta \tag{11}$$

equation (10) can be rewritten as:

$$\int_\Omega \sqrt{\det \mathbf{g}}\, \bar{e}\, \eta dV - \int_{\partial\Omega} c\sqrt{\det \mathbf{g}}\, \eta\, (\mathbf{g}^{-1} \cdot \nabla \bar{e}) \cdot \boldsymbol{n} dS + \int_\Omega c(\sqrt{\det \mathbf{g}}\, \mathbf{g}^{-1} \cdot \nabla \bar{e}) \cdot \nabla \eta dV = \int_\Omega \sqrt{\det \mathbf{g}} e\eta dV \ \ \forall \eta \in \mathcal{V} \tag{12}$$

Substituting in the integral equation above and taking into account for the Neumann zero flux condition (4), one obtains the final problem to be solved. It consists in finding at each time t the field $\bar{e} \in \mathcal{V}$ satisfying:[1]

$$\int_\Omega \sqrt{\det \mathbf{g}}\, \bar{e}\, \eta dV + \int_\Omega (c\sqrt{\det \mathbf{g}}\, \mathbf{g}^{-1} \cdot \nabla \bar{e}) \cdot \nabla \eta dV = \int_\Omega \sqrt{\det \mathbf{g}}\, e\, \eta dV \ \ \forall \eta \in \mathcal{V} \tag{14}$$

[1] The variational formulation of the GNL model (Peerlings et al., 1996) is retrieved by considering $\mathbf{g} = \mathbf{g}^{-1} = \mathbf{I}$, such as:

$$\int_\Omega \bar{e}\eta dV + \int_\Omega c\nabla \bar{e} \cdot \nabla \eta dV = \int_\Omega e\eta dV \ \ \forall \eta \in V \tag{13}$$

3. Standard thermodynamics derivations of the ENLG model based on a postulated free-energy

Starting from a free-energy potential inspired to the one proposed by Peerlings et al. (2004) for deriving the GNL model, this section illustrates a standard way of obtaining the governing equations of the ENLG model. The method is based on the formalism presented by Forest (2009) for micromorphic media. It is shown that non-locality comes into the picture in the expression of the stress tensor (even in elastic conditions) and affects the intrinsic dissipation. This latter can no more be computed using the standard expression valid for local models, as for the GNL model. Some conclusions concerning the Cauchy stress tensor definition and the fulfillment of the Clausius-Duhem inequality are finally drawn to motivate the differential geometry thermodynamics description introduced in the next section.

3.1. Derivation of the anisotropic model from the micromorphic media approach

Following the so-called "micromorphic media theory" (Forest, 2009), $\bar{e}$ is taken as the micromorphic variable, while e is its equivalent macro quantity. As a result, $\boldsymbol{u}$ and $\bar{e}$ are the unknown of the problem.

Extended virtual power principle. Neglecting contact and volume forces, the virtual power principle reads:

$$\mathcal{P}^*_{\text{int}}(\boldsymbol{v}^*, \dot{\eta}^*) + \mathcal{P}^*_{\text{ext}}(\boldsymbol{v}^*, \dot{\eta}^*) = 0 \quad \forall\, \boldsymbol{v}^*, \dot{\eta}^* \tag{15}$$

where $\boldsymbol{v}^*$ and $\dot{\eta}^*$ are the virtual velocity and the virtual variation rate of $\bar{e}$, respectively. The generalized virtual powers of the internal ($\mathcal{P}^*_{\text{int}}$) and external ($\mathcal{P}^*_{\text{ext}}$) forces read:

$$\mathcal{P}^*_{\text{int}}(\boldsymbol{v}^*, \dot{\eta}^*) = -\int_\Omega \underbrace{\left(\boldsymbol{\sigma} : \boldsymbol{\epsilon}(\boldsymbol{v}^*) + a\dot{\eta}^* + \boldsymbol{b}\cdot\nabla\dot{\eta}^*\right)}_{:=p^{(i)}(\boldsymbol{v}^*,\dot{\eta}^*)} dV \tag{16}$$

$$\mathcal{P}^*_{\text{ext}}(\boldsymbol{v}^*, \dot{\eta}^*) = \int_\Omega \left(a^e\dot{\eta}^* + \boldsymbol{b}^e\cdot\nabla\dot{\eta}^*\right) dV + \int_{\partial\Omega} \left(\boldsymbol{t}^d\cdot\boldsymbol{v}^* + a^c\dot{\eta}^*\right) dS \tag{17}$$

where a and $\boldsymbol{b}$ are generalized stresses related to the micromorphic variable and its first gradient, a^e and $\boldsymbol{b}^e$ are the generalized body forces, and a^c are the generalized tractions applied on the boundary $\partial\Omega$.

Exploiting the arbitrary nature of the virtual velocity fields $(\boldsymbol{v}^*, \dot{\eta}^*)$, one obtains the momentum balance equations and the corresponding boundary conditions:

$$\nabla\cdot\boldsymbol{\sigma} = \boldsymbol{0} \qquad \text{on}\,\Omega \tag{18}$$

$$\nabla\cdot(\boldsymbol{b} - \boldsymbol{b}^e) - a + a^e = 0 \qquad \text{on}\,\Omega \tag{19}$$

$$\boldsymbol{t}^d = \boldsymbol{\sigma}\cdot\boldsymbol{n} \qquad \text{on}\,\partial\Omega \tag{20}$$

$$a^c = (\boldsymbol{b} - \boldsymbol{b}^e)\cdot\boldsymbol{n} \qquad \text{on}\,\partial\Omega \tag{21}$$

Entropy principle. Under isothermal conditions, the entropy principle reads:

$$p^{(i)} - \rho\dot{\psi} = \boldsymbol{\sigma} : \boldsymbol{\epsilon} + a\dot{\bar{e}} + \boldsymbol{b} \cdot \nabla\dot{\bar{e}} - \rho\dot{\psi} \geq 0. \tag{22}$$

where the free energy potential ψ is considered to be a function of the micromorphic quantities and their gradients. For a anisotropic damage model with a second order tensorial damage variable one has:

$$\rho\psi = \rho\psi(\boldsymbol{\epsilon}, \mathbf{D}, \bar{e}, \nabla\bar{e}) \tag{23}$$

Computing the derivative of the potential with respect to time gives:

$$\rho\dot{\psi} = \rho\frac{\partial\psi}{\partial\boldsymbol{\epsilon}} : \dot{\boldsymbol{\epsilon}} + \rho\frac{\partial\psi}{\partial\mathbf{D}} : \dot{\mathbf{D}} + \rho\frac{\partial\psi}{\partial\bar{e}}\dot{\bar{e}} + \rho\frac{\partial\psi}{\partial\nabla\bar{e}}\nabla\dot{\bar{e}} \tag{24}$$

and replacing this expression into (22), one has:

$$\left(\boldsymbol{\sigma} - \rho\frac{\partial\psi}{\partial\boldsymbol{\epsilon}}\right) : \dot{\boldsymbol{\epsilon}} + \left(a - \rho\frac{\partial\psi}{\partial\bar{e}}\right)\dot{\bar{e}} + \left(\boldsymbol{b} - \rho\frac{\partial\psi}{\partial\nabla\bar{e}}\right)\nabla\dot{\bar{e}} - \rho\frac{\partial\psi}{\partial\mathbf{D}} : \dot{\mathbf{D}} \geq 0 \tag{25}$$

The following state laws can therefore be derived:

$$\boldsymbol{\sigma} = \rho\frac{\partial\psi}{\partial\boldsymbol{\epsilon}} \quad \mathbf{Y} = -\rho\frac{\partial\psi}{\partial\mathbf{D}} \quad a = \rho\frac{\partial\psi}{\partial\bar{e}} \quad \boldsymbol{b} = \rho\frac{\partial\psi}{\partial\nabla\bar{e}} \tag{26}$$

Thermodynamic potential. Drawing from the free-energy potential postulated by Peerlings et al. (2004) for deriving the standard isotropic GNL model, a free-energy potential for the anisotropic ENLG model can be written as:

$$\rho\psi = \rho\psi(\boldsymbol{\epsilon}, \mathbf{D}, \bar{e}) = \rho\psi_0 + \frac{1}{2}h\sqrt{\det\mathbf{g}}\,(e - \bar{e})^2 + \frac{1}{2}hc\sqrt{\det\mathbf{g}}\,\mathbf{g}^{-1} : (\nabla\bar{e} \otimes \nabla\bar{e}) \tag{27}$$

where $\rho\psi_0 = \rho\psi_0(\boldsymbol{\epsilon}, \mathbf{D})$ is the free-energy potential postulated by the anisotropic damage model (see e.g., (Desmorat et al., 2007; Desmorat, 2015; Masseron et al., 2022)), $h > 0$ is a model parameter (homogeneous to a stiffness), and $\otimes$ denotes the standard tensor product.[2]

Model equations. The expression of the stress tensor, the Helmholtz damage diffusion equation and the intrinsic dissipation can be obtained by applying these state laws, such as:

(*i*) The stress tensor $\boldsymbol{\sigma}$ reads as the sum of a standard contribution ($\boldsymbol{\sigma}_0$) and a damage-dependent term related to non-locality:

$$\boldsymbol{\sigma} = \boldsymbol{\sigma}_0 + h\sqrt{\det\mathbf{g}}(e - \bar{e})\frac{\partial e}{\partial\boldsymbol{\epsilon}} \tag{29}$$

[2]Given three vectors ($\boldsymbol{a}$, $\boldsymbol{b}$, $\boldsymbol{c}$), the tensor product $\boldsymbol{a} \otimes \boldsymbol{b}$ is defined as:

$$(\boldsymbol{a} \otimes \boldsymbol{b}) \cdot \boldsymbol{c} = (\boldsymbol{b} \cdot \boldsymbol{c})\boldsymbol{a} \qquad (\boldsymbol{a} \otimes \boldsymbol{b})_{ij} = a_i b_j \tag{28}$$

Compared to (Peerlings et al., 2004), the additional damage-dependent factor $\sqrt{\det \mathbf{g}}$ is present in (29). The formulation of Peerlings et al. (2004) is recovered in undamaged conditions (i.e., $\mathbf{D} = \mathbf{0}$) since $\mathbf{g} = \mathbf{I}$ and $\det \mathbf{g} = 1$.

(*ii*) The terms a and b read:

$$a = -h\sqrt{\det \mathbf{g}}(e - \bar{e}) \qquad \boldsymbol{b} = hc\sqrt{\det \mathbf{g}}(\mathbf{g}^{-1} \cdot \nabla \bar{e}) \tag{30}$$

Introducing the usual assumption (Forest, 2009) of no generalized volume forces ($a^e = 0, \boldsymbol{b}^e = \mathbf{0}$), equations (19) and (21) give:

$$\sqrt{\det \mathbf{g}}\,(e - \bar{e}) - c\nabla \cdot (\sqrt{\det \mathbf{g}}\,\mathbf{g}^{-1} \cdot \nabla \bar{e}) = 0 \qquad \text{on } \Omega \tag{31}$$

$$\mathbf{g}^{-1} \cdot \nabla \bar{e} \cdot \boldsymbol{n} = 0 \qquad \text{on } \partial\Omega \tag{32}$$

where, to simplify the boundary condition, we exploited the condition $\det \mathbf{g} > 0$.

(*iii*) The intrinsic dissipation is:

$$\mathcal{D} = \mathbf{Y} : \dot{\mathbf{D}} \tag{33}$$

where the thermodynamic force associated with damage $\mathbf{Y}$ reads:

$$\mathbf{Y} = \mathbf{Y}(\boldsymbol{\epsilon}, \mathbf{D}, \bar{e}) = \mathbf{Y}_0 + \mathbf{Z} = -\rho\frac{\partial \psi_0}{\partial \mathbf{D}} + \mathbf{Z} \tag{34}$$

The tensorial function $\mathbf{Z}$ can be understood as a non-local rate of energy restitution of the model. Such an additional non-local term does not appear in the case of the GNL model (Peerlings et al., 2004). As already mentioned, in this case the dissipation does not differ from the one corresponding to the local model.

3.2. Isotropic ENLG model as a special case

Simplified two- (2D) and three-dimensional (3D) isotropic damage mechanics formulations can be obtained by considering specific metrics. In the following, the 3D, full 2D, plane-stress, and plane-strain problems are treated separately for completeness.

3.2.1. 3D conditions

The isotropic 3D Helmholtz problem to be solved can be derived considering $\mathbf{D} = D\mathbf{I}$, such as the metric tensor reads:

$$\mathbf{g} = \frac{\mathbf{I}}{1 - D} \tag{35}$$

Observing that:

$$\det \mathbf{g} = \frac{1}{(1-D)^3} \quad \mathbf{g}^{-1} = (1 - D)\mathbf{I} \quad \sqrt{\det \mathbf{g}}\,\mathbf{g}^{-1} = \frac{1}{\sqrt{1 - D}}\mathbf{I} \tag{36}$$

equations (3) and (4) can be simplified as:

$$\bar{e} - c\sqrt{(1-D)^3}\nabla\cdot\left(\frac{1}{\sqrt{1-D}}\nabla\bar{e}\right) = e \qquad \text{on}\,\Omega \tag{37}$$

$$\nabla\bar{e}\cdot\boldsymbol{n} = 0 \qquad \text{on}\,\partial\Omega \tag{38}$$

where we exploited the condition $1-D>0$ to simplify the Neumann boundary condition. The variational equation to be solved thus reads:

$$\int_\Omega \frac{1}{\sqrt{(1-D)^3}}\,\bar{e}\,\eta dV + \int_\Omega \frac{c}{\sqrt{1-D}}\nabla\bar{e}\cdot\nabla\eta dV = \int_\Omega \frac{1}{\sqrt{(1-D)^3}}\,e\,\eta dV \;\;\forall\eta\in\mathcal{V} \tag{39}$$

This formulation can also be easily derived according to the procedures described before, by considering, the following free-energy potential:

$$\rho\psi = \rho\psi(\boldsymbol{\epsilon}, D, \bar{e}) = \rho\psi_0(\boldsymbol{\epsilon}, D\mathbf{I}) + \frac{1}{2}h\frac{1}{\sqrt{(1-D)^3}}\left(e-\bar{e}\right)^2 + \frac{1}{2}hc\frac{1}{\sqrt{1-D}}\nabla\bar{e}\cdot\nabla\bar{e} \tag{40}$$

where we employed the property $\mathbf{I}:(\nabla\bar{e}\otimes\nabla\bar{e}) = \mathrm{tr}(\nabla\bar{e}\otimes\nabla\bar{e}) = \nabla\bar{e}\cdot\nabla\bar{e}$.

From the state laws, one obtains the following expressions for the Cauchy stress tensor:

$$\boldsymbol{\sigma} = \boldsymbol{\sigma}_0 + h\frac{1}{\sqrt{(1-D)^3}}(e-\bar{e})\frac{\partial e}{\partial\boldsymbol{\epsilon}} \tag{41}$$

and for the (scalar) thermodynamic force associated with damage:

$$Y = Y_0 + Z \tag{42}$$

Here:

$$Y_0 = -\rho\frac{\partial\psi_0}{\partial(D\mathbf{I})}:\mathbf{I} = -3\rho\frac{\partial\psi_0}{\partial D} \geq 0 \tag{43}$$

$$\begin{aligned} Z &= -\frac{h}{2}\frac{\partial}{\partial D}\left[\frac{1}{\sqrt{(1-D)^3}}\left(e-\bar{e}\right)^2 + \frac{c}{\sqrt{1-D}}\nabla\bar{e}\cdot\nabla\bar{e}\right] \\ &= -\frac{h}{2}\left[\frac{3}{2}\frac{1}{\sqrt{(1-D)^5}}\left(e-\bar{e}\right)^2 + \frac{c}{(1-D)^2}\nabla\bar{e}\cdot\nabla\bar{e}\right] \leq 0 \end{aligned} \tag{44}$$

One also obtains:

$$a = -\frac{h}{\sqrt{(1-D)^3}}(e-\bar{e}) \tag{45}$$

$$\boldsymbol{b} = \frac{hc}{\sqrt{1-D}}\nabla\bar{e} \tag{46}$$

3.2.2. 2D conditions

The full 2D isotropic Helmholtz problem to be solved can be derived with:

$$\mathbf{g} = \frac{\mathbf{I_2}}{1-D} \tag{47}$$

with $\mathbf{I_2}$ denoting the 2D identity tensor. In this case, $\Omega \subset \mathbb{R}^2$ and:

$$\det \mathbf{g} = \frac{1}{(1-D)^2} \quad \mathbf{g}^{-1} = (1-D)\mathbf{I_2} \quad \sqrt{\det \mathbf{g}}\,\mathbf{g}^{-1} = \mathbf{I_2} \tag{48}$$

As a consequence, equations (3) and (4) can be simplified as:

$$\bar{e} - c(1-D)\nabla \cdot \nabla \bar{e} = e \qquad \text{on } \Omega \tag{49}$$

$$\nabla \bar{e} \cdot \boldsymbol{n} = 0 \qquad \text{on } \partial\Omega \tag{50}$$

The variational problem to be solved is:

$$\int_\Omega \frac{1}{1-D}\,\bar{e}\,\eta dV + \int_\Omega c\nabla\bar{e}\cdot\nabla\eta dV = \int_\Omega \frac{1}{1-D}\,e\,\eta dV \;\; \forall \eta \in \mathcal{V} \tag{51}$$

The following free-energy potential can be considered to derive the 2D isotropic ENLG damage formulation:

$$\rho\psi = \rho\psi(\boldsymbol{\epsilon}, D, \bar{e}) = \rho\psi_0(\boldsymbol{\epsilon}, D\mathbf{I_2}) + \frac{1}{2}\frac{h}{1-D}\left(e-\bar{e}\right)^2 + \frac{1}{2}hc\nabla\bar{e}\cdot\nabla\bar{e} \tag{52}$$

By applying the state laws, one obtains the following expression of the Cauchy stress tensor:

$$\boldsymbol{\sigma} = \boldsymbol{\sigma}_0 + \frac{h}{1-D}(e-\bar{e})\frac{\partial e}{\partial \boldsymbol{\epsilon}} \tag{53}$$

The thermodynamic force Y reads as in (42), with Y_0 defined as in (43) and:

$$Z = -\frac{h}{2}\frac{\partial}{\partial D}\left[\frac{1}{1-D}\left(e-\bar{e}\right)^2\right] = -\frac{h}{4}\frac{1}{(1-D)^2}\left(e-\bar{e}\right)^2 \leq 0 \tag{54}$$

In addition to equations (53), (42), (43) and (54), one also obtains:

$$a = -\frac{h}{1-D}(e-\bar{e}) \tag{55}$$

$$\boldsymbol{b} = hc\nabla\bar{e} \tag{56}$$

Plane-stress and plane-strain conditions. The equations introduced above can be used to address the situations of plane-stress and plane-strain. Specifically, in the case of plane-strain conditions, the complete 2D equations are still applicable since the out-of-plane strain is non-null and the out-of-plane component of $\nabla\bar{e}$ is assumed null.

3.3. Comments on stress tensor and energy dissipation

Although the boundary value problem corresponding to the ENLG model could be derived from the proposed potential, one can detect some inconsistencies in the previous formulations by investigating the expressions of the stress tensor and the intrinsic dissipation for the isotropic case. In particular:

(*i*) *Stress tensor.* Let us analyze equations (41) and (53). Contrarily to the GNL model, the term $(1-D)$ figures at the denominator of the non-local contributions. It results from the "arbitrary" modification of the free-energy potential by Peerlings et al. (2004) to account for damage-dependent interactions. Now, the term $(1-D)\mathbb{E}:\boldsymbol{\epsilon}$ vanishes when $D \to 1$ but this is not the case of the second contributions of both equations. If an arbitrary small constant value is chosen for h, the second contributions to $\boldsymbol{\sigma}$ in equations (41) and (53) may eventually tend to infinity when $D \to 1$. This is physically inconsistent since a zero-stress condition should be described.

(*ii*) *Energy dissipation.* Let us now consider equations (44) and (54). A first remark is that the expressions of Z differ depending on the problem dimension (i.e., the energy dissipation depends on the problem dimension). Besides that, it has been shown that Z is always negative. Consequently, the dissipation inequality $(Y_0+Z)\dot{D} \geq 0$ may not be verified in some situations. This is the case when $D \to 1$ since the term $(1-D)$ figures at the denominator of both expressions of Z. The Clausius-Duhem inequality is, therefore, not fulfilled.

The inconsistencies mentioned above are intrinsically related to how the modified free-energy potentials (40) and (52) were written. To obtain the Helmholtz equation corresponding to the ENLG model, the factor $\sqrt{\det \mathbf{g}}$ was added to the terms related to the non-local strain and its gradient. However, this led to a wrong description of the stress tensor and intrinsic dissipation. In other words, such a way of defining the free-energy potential does not allow for correctly deriving the ENLG model. A different point of view needs to be introduced to achieve this objective.

4. Differential geometry viewpoint to the thermodynamics of ENLG models

This section gives the first insights into a possible thermodynamics framework to derive the ENLG model. A geometric description is introduced using differential geometry concepts. Two different spaces are used in the eikonal problem. A Euclidean space, where Ω is placed in a given configuration, and a Riemannian space, where non-local interactions are computed. In the latter case, a tangent space is defined at each point of an abstract differentiable manifold $\mathcal{M}$ (i.e., a topological manifold with a globally defined differential structure), where the metric $\mathbf{g}$ defines a scalar product. To derive the formulation, the non-local equivalent

strain is seen as a morphological descriptor and is an element of $\mathcal{M}$ (see (Mariano and Stazi, 2005) for further discussions). This idea directly stems from the theoretical assumption that damage curves the space where the non-local interactions are computed (Desmorat et al., 2015). Similar ideas were presented in (Ganghoffer and de Borst, 2000; Ganghoffer, 2003), where a metric was coupled with an internal variable distribution. In their work, the strength of interactions is incorporated into the space's geometry, such as their effect on the curvature is discussed. Other contributions where geometric concepts are used to describe damage behaviors exist (e.g., (Steinmann and Carol, 1998; Mariano, 2010; Das et al., 2021)).

4.1. A few useful elements of differential geometry

In curved spaces, contravariant and covariant coordinates differ. The basic rules are: (*i*) if $\boldsymbol{a}$ is a vector living in a vectorial space E, then its coordinates are represented by a^i (with upper index); (*ii*) if $\boldsymbol{a}$ is a covector living in the dual space E^*, then its coordinates are represented by a_i (with lower index); (*iii*) metric tensors are totally symmetric (and positive definite) second-order tensors of covariant nature. Tensor $\mathbf{g} : \mathrm{E} \to \mathrm{E}^*$ is represented by its covariant components g_{ij} and $\mathrm{g}_{ik}\mathrm{g}^{kj} = \delta_i{}^j$, which is the mixed second order identity tensor; (*iv*) only upper and lower indexes can be contracted; (v) the covector associated with vector $\boldsymbol{a}$ is given by:

$$\boldsymbol{a}^{\#} = \mathbf{g} \cdot \boldsymbol{a} \qquad (a^{\#})_i = \mathrm{g}_{ij} a^j \tag{57}$$

whereas the vector associated with covector $\boldsymbol{b}$ is given by:

$$\boldsymbol{b}^{\flat} = \mathbf{g}^{-1} \cdot \boldsymbol{b} \qquad (b^{\flat})^i = \mathrm{g}^{ij} b_j \tag{58}$$

Scalar product. A scalar product between two covectors $\boldsymbol{b}$ and $\boldsymbol{c}$ is defined by a metric contraction as:

$$\langle \boldsymbol{b}, \boldsymbol{c} \rangle_{\mathbf{g}} := \boldsymbol{b} \cdot \boldsymbol{c}^{\flat} = \boldsymbol{b} \cdot \mathbf{g}^{-1} \cdot \boldsymbol{c} = \mathbf{g}^{-1} : (\boldsymbol{b} \otimes \boldsymbol{c}) = b_i \mathrm{g}^{ij} c_j \tag{59}$$

In the Riemannian space curved by damage, the metric and its inverse read:

$$\mathbf{g} = (\mathbf{q} - \mathbf{D})^{-1} \qquad g_{ij} = [(\mathbf{q} - \mathbf{D})^{-1}]_{ij} \tag{60}$$

$$\mathbf{g}^{-1} = \mathbf{q}^{-1} - \mathbb{I}^{\flat} : \mathbf{D} \qquad g^{ij} = q^{ij} - I^{ijkl} D_{kl} \tag{61}$$

where $\mathbf{q} = \mathbf{I} = \delta_{ij}$ and $\mathbb{I}^{\flat} : \mathrm{E}^* \times \mathrm{E}^* \to \mathrm{E} \times \mathrm{E}$ is the Euclidean 4th-order identity tensor:

$$\mathbb{I}^{\flat} = \mathbf{q}^{-1} \,\overline{\otimes}\, \mathbf{q}^{-1} \qquad I^{ijkl} = \frac{1}{2}\left(q^{ik} q^{jl} + q^{il} q^{jk}\right) \tag{62}$$

where $\overline{\otimes}$ denotes the symmetrized tensor product. According to previous definition, tensor $\mathbb{I}^{\flat}$ transforms Euclidean covariant tensors into an Euclidean contravariant tensors.[3] Similarly, the tensor $\mathbb{I}_{\#} : \mathrm{E} \times \mathrm{E} \to$

[3] Given a covariant tensor $\mathbf{T} \in \mathrm{E}^* \times \mathrm{E}^*$, one has:

$$\mathbf{T}^{\flat} = \mathbb{I}^{\flat} : \mathbf{T} \qquad T^{ij} = I^{ijkl} T_{kl} \tag{63}$$

$\mathrm{E}^* \times \mathrm{E}^*$:[4]

$$\mathbb{I}_{\#} = \mathbf{q} \,\overline{\otimes}\, \mathbf{q} \qquad I_{ijkl} = \frac{1}{2}\left(q_{ik}q_{jl} + q_{il}q_{jk}\right) \tag{65}$$

transforms Euclidean contravariant tensors into an Euclidean covariant tensors. The mixed fourth-order identity tensor $\mathbb{I}^{\flat}_{\#} : \mathrm{E} \times \mathrm{E} \to \mathrm{E} \times \mathrm{E}$:[5]

$$\mathbb{I}^{\flat}_{\#} = \mathbb{I}^{\flat} : \mathbb{I}_{\#} \qquad I^{ij}_{\ \ mn} = I^{ijkl} I_{klmn} \tag{67}$$

transforms contravariant tensors into themselves. Finally, the conjugated mixed fourth-order identity tensor $\mathbb{I}^{\ \flat}_{\#} : \mathrm{E}^* \times \mathrm{E}^* \to \mathrm{E}^* \times \mathrm{E}^*$:[6]

$$\mathbb{I}^{\ \flat}_{\#} = \mathbb{I}_{\#} : \mathbb{I}^{\flat} \qquad I_{ij}^{\ \ mn} = I_{ijkl} I^{klmn} \tag{69}$$

transforms covariant tensors into themselves.

In the Euclidean space or undamaged medium, one has:

$$\mathbf{g} = \mathbf{q} = \mathbf{I} = \delta_{ij} \qquad \mathbf{g}^{-1} = \mathbf{q}^{-1} = \mathbf{I}^{-1} = \delta^{ij} \tag{70}$$

i.e., the covariant and contravariant Euclidean metrics, so that (59) defines the standard scalar product. Based on this description, the isotropic elasticity law can be rewritten as:

$$\boldsymbol{\sigma} = 2\mu \mathbb{I}^{\flat} : \boldsymbol{\epsilon} + \lambda \mathrm{Tr}(\mathbf{q}^{-1} \cdot \boldsymbol{\epsilon}) \mathbf{q}^{-1} \qquad (\boldsymbol{\sigma})^{ij} = 2\mu q^{ik} (\boldsymbol{\epsilon})_{kl} q^{jl} + \lambda (\boldsymbol{\epsilon})^k_k q^{ij} \tag{71}$$

with μ and λ denoting the two Lamé parameters. Notice that according to previous equation $\boldsymbol{\epsilon}$ is a covariant tensor whereas $\boldsymbol{\sigma}$ is a contravariant tensor.

Gradient of a function. In local coordinates (x^i), $(\partial/\partial x^i = \partial_i)$ denotes the basis of the tangent space $\mathrm{T}_{\boldsymbol{x}}\mathcal{M}$ and dx^i is the dual basis of the cotangent space $\mathrm{T}^{\star}_{\boldsymbol{x}}\mathcal{M}$ for $\boldsymbol{x} \in \mathcal{M}$ (it is such that $dx^i(\partial_j) = \delta^i_j$).

The derivative df of a function $f : \mathcal{M} \to \mathbb{R}$ is the 1-form of covariant components $df_i = \partial_i f$. The gradient of f is therefore the vector obtained as:

$$\nabla f = \mathbf{g}^{-1} \cdot df \quad (\nabla f)^i = \partial^i f = \mathrm{g}^{ij} \partial_j f \tag{72}$$

[4]Given a contravariant second order tensor $\mathbf{S} \in \mathrm{E} \times \mathrm{E}$ one has:

$$\mathbf{S}_{\#} = \mathbb{I}_{\#} : \mathbf{S} \qquad S_{ij} = I_{ijkl} S^{kl} \tag{64}$$

[5]Given a contravariant second order tensor $\mathbf{S} \in \mathrm{E} \times \mathrm{E}$ one has:

$$\mathbf{S} = \mathbb{I}^{\flat}_{\#} : \mathbf{S} \qquad S^{ij} = I^{ij}_{\ \ mn} S^{mn} \tag{66}$$

[6]Given a covariant second order tensor $\mathbf{T} \in \mathrm{E}^* \times \mathrm{E}^*$ one has:

$$\mathbf{T} = \mathbb{I}^{\ \flat}_{\#} : \mathbf{T} \qquad T_{ij} = I_{ij}^{\ \ mn} T_{mn} \tag{68}$$

In the case of Euclidean spaces, one has $\nabla f = (\nabla f)^i = \delta^{ij}\partial_j f = \partial_i f = (df)_i = df$, so the gradient ∇f and the 1-form df do not differ.

The Riemannian norm $\|\nabla f\|_{\mathbf{g}}$ is defined as:

$$\|\nabla f\|^2_{\mathbf{g}} = \langle \nabla f, \nabla f\rangle_{\mathbf{g}} = \nabla f \cdot \mathbf{g} \cdot \nabla f = df \cdot \mathbf{g}^{-1} \cdot df = \langle df, df\rangle_{\mathbf{g}} = \|df\|^2_{\mathbf{g}} \tag{73}$$

Laplacian of a function. The divergence of the gradient on a manifold is the so-called "connection Laplacian" or "Laplace-Beltrami operator". It is defined as:

$$\Delta f := \nabla \cdot \nabla f = \frac{1}{\sqrt{\det(\mathrm{g}_{ij})}}\partial_i \left(\sqrt{\det(\mathrm{g}_{ij})}\mathrm{g}^{ij}\partial_j f \right). \tag{74}$$

In Euclidean spaces, the Laplace-Beltrami operator generalizes the usual Laplacian definition, i.e., $\Delta f = \partial_i\partial_i f = \nabla \cdot (\nabla f)$.

4.2. Anisotropic ENLG model

Let us suppose that the non-local equivalent strain is a map (i.e., a linear application from the manifold to the real space, $\bar{e} : \mathcal{M} \to \mathbb{R}$). The free-energy potential can directly be written on the manifold as:

$$\rho\psi = \rho\psi(\boldsymbol{\epsilon}, \mathbf{D}, \bar{e}, \tilde{\nabla}\bar{e}) = \rho\psi_0 + \frac{1}{2}h(e-\bar{e})^2 + \frac{1}{2}hc\|\tilde{\nabla}\bar{e}\|^2_{\mathbf{g}} \tag{75}$$

where, to avoid confusion, the symbol $\tilde{\nabla}$ is now used to denote that the gradient (and also the divergence in the remainder of this section) is computed in the deformed space by damage (i.e., on the manifold $\mathcal{M}$). Given this choice, the factors $\sqrt{\det\mathrm{g}}$ no longer appear in the expression of $\rho\psi$ (se eq.(27)).

State laws. The state laws read:

$$\boldsymbol{\sigma} = \boldsymbol{\sigma}_0 + h(e-\bar{e})\frac{\partial e}{\partial \boldsymbol{\epsilon}} \qquad \sigma^{ij} = \sigma_0^{ij} + h(e-\bar{e})\left(\frac{\partial e}{\partial \boldsymbol{\epsilon}}\right)^{ij} \tag{76}$$

$$\mathbf{Y} = \mathbf{Y}_0 + \mathbf{Z} \qquad Y^{ij} = Y_0^{ij} + Z^{ij} \tag{77}$$

$$a = -h(e-\bar{e}) \tag{78}$$

$$\boldsymbol{b} = \rho\frac{\partial \psi}{\partial \tilde{\nabla}\bar{e}} = hc\mathbf{g}\cdot\tilde{\nabla}\bar{e} \qquad b_i = hc\mathrm{g}_{ij}(\tilde{\nabla}\bar{e})^j = hc(d\bar{e})_i = hc\partial_i\bar{e} \tag{79}$$

where:

$$\boldsymbol{\sigma}_0 = \rho\frac{\partial \psi_0(\boldsymbol{\epsilon}, \mathbf{D})}{\partial \boldsymbol{\epsilon}} \qquad \sigma_0^{ij} = \left(\rho\frac{\partial \psi_0(\boldsymbol{\epsilon}, \mathbf{D})}{\partial \boldsymbol{\epsilon}}\right)^{ij} \tag{80}$$

$$\mathbf{Y}_0 = -\rho\frac{\partial \psi_0(\boldsymbol{\epsilon}, \mathbf{D})}{\partial \mathbf{D}} \qquad Y_0^{ij} = -\left(\rho\frac{\partial \psi_0(\boldsymbol{\epsilon}, \mathbf{D})}{\partial \mathbf{D}}\right)^{ij} \tag{81}$$

$$\mathbf{Z} = -\frac{hc}{2}\frac{\partial\|d\bar{e}\|^2_{\mathbf{g}}}{\partial \mathbf{g}^{-1}} : \frac{\partial \mathbf{g}^{-1}}{\partial \mathbf{D}} \qquad Z^{ij} = -\frac{hc}{2}\left(\frac{\partial\|d\bar{e}\|^2_{\mathbf{g}}}{\partial \mathbf{g}^{-1}}\right)_{kl}\left(\frac{\partial \mathbf{g}^{-1}}{\partial \mathbf{D}}\right)^{klij} \tag{82}$$

One can notice that the expression of the thermodynamic forces are naturally contravariant by simple derivation and index contraction rules, for instance:

$$\rho\partial\psi_0(\boldsymbol{\epsilon},\mathbf{D}) = \left(\rho\frac{\partial\psi_0(\boldsymbol{\epsilon},\mathbf{D})}{\partial\boldsymbol{\epsilon}}\right)^{ij}\partial\epsilon_{ij} + \left(\rho\frac{\partial\psi_0(\boldsymbol{\epsilon},\mathbf{D})}{\partial\mathbf{D}}\right)^{ij}\partial D_{ij} \tag{83}$$

Helmholtz equation. From the balance equation (19), one has:

$$\tilde{\nabla}\cdot\boldsymbol{b}^\flat - a = 0 \tag{84}$$

where a^c was supposed null and $\boldsymbol{b}^\flat$ is the vector associated with the covector $\boldsymbol{b}$:

$$\boldsymbol{b}^\flat = hc\mathbf{g}^{-1}\cdot\boldsymbol{b} = hc\tilde{\nabla}\bar{e} \qquad (\boldsymbol{b})^{\flat,i} = hc\mathrm{g}^{ij}\partial_j\bar{e} \tag{85}$$

Replacing (85) into (84) one obtains:

$$\tilde{\nabla}\cdot(hc\tilde{\nabla}\bar{e}) - h\bar{e} + he = 0 \tag{86}$$

and then, exploiting the fact that h and c are both constant and non-null:

$$\bar{e} - c\tilde{\nabla}\cdot\left(\tilde{\nabla}\bar{e}\right) = e \tag{87}$$

The same expression was obtained in (Desmorat et al., 2015). Previous equation can also be written in an euclidean space as:

$$\bar{e} - \frac{c}{\sqrt{\det\mathbf{g}}}\nabla\cdot(\sqrt{\det\mathbf{g}}\,\mathbf{g}^{-1}\cdot\nabla\bar{e}) = e. \tag{88}$$

where $\nabla\bar{e}$ is taken here equal to the 1-form $\partial_i\bar{e} = d\bar{e}_i$.

Variational formulation. A variational formulation for the ENLG model can be obtained directly starting from equation (87).[7] One has:

$$\int_{\mathcal{M}}\bar{e}\eta\mathrm{vol}_g - \int_{\mathcal{M}}c\tilde{\nabla}\cdot\left(\tilde{\nabla}\bar{e}\right)\eta\mathrm{vol}_g = \int_{\mathcal{M}}e\eta\mathrm{vol}_g. \tag{89}$$

where:

$$c\tilde{\nabla}\cdot\left(\tilde{\nabla}\bar{e}\eta\right) = c\tilde{\Delta}\bar{e}\eta + c\langle\tilde{\nabla}\bar{e},\tilde{\nabla}\eta\rangle_{\mathbf{g}} \tag{90}$$

and:

$$\mathrm{vol}_g = \sqrt{\det(\mathrm{g}_{ij})}dx^1\wedge dx^2...\wedge dx^n \tag{91}$$

a n-form (the volume form). In previous equation $\wedge$ denotes the vector product. The above integral thus becomes:

$$\int_{\mathcal{M}}\bar{e}\eta\mathrm{vol}_g - \int_{\mathcal{M}}c\tilde{\nabla}\cdot\left(\tilde{\nabla}\bar{e}\eta\right)\mathrm{vol}_g + \int_{\mathcal{M}}c\langle\tilde{\nabla}\bar{e},\tilde{\nabla}\eta\rangle_{\mathbf{g}}\mathrm{vol}_g = \int_{\mathcal{M}}e\eta\mathrm{vol}_g \tag{92}$$

[7] Alternatively, one could use the micromorphic approach by writing the principle of virtual work in the curved space.

Applying the divergence theorem:

$$\int_{\mathcal{M}} c\tilde{\nabla}\cdot\left(\tilde{\nabla}\bar{e}\eta\right)\mathrm{vol}_g = \int_{\partial\mathcal{M}} c\eta(\tilde{\nabla}\bar{e}\cdot\mathbf{g})\cdot\boldsymbol{n}dS \tag{93}$$

enforcing the boundary condition:

$$(\tilde{\nabla}\bar{e}\cdot\mathbf{g})\cdot\boldsymbol{n} = 0 \quad \text{on}\,\partial\mathcal{M} \tag{94}$$

and remembering that $\langle\tilde{\nabla}\bar{e},\tilde{\nabla}\eta\rangle_{\mathbf{g}} = \langle d\bar{e},d\eta\rangle_{\mathbf{g}}$ (see equation (73)), one ends up with:

$$\int_{\mathcal{M}}\bar{e}\eta\mathrm{vol}_g + \int_{\mathcal{M}} c\langle d\bar{e},d\eta\rangle_{\mathbf{g}}\mathrm{vol}_g = \int_{\mathcal{M}} e\eta\mathrm{vol}_g. \tag{95}$$

Here, $(d\bar{e})_i = \partial_i\bar{e}$ denotes the 1-form, which is usually taken as the gradient in Euclidean space. Consequently, a straightforward rewriting of last variational equation is:

$$\int_\Omega \sqrt{\mathrm{detg}}\bar{e}\eta dV + \int_\Omega c\sqrt{\mathrm{detg}}(\mathbf{g}^{-1}\cdot\nabla\bar{e})\cdot\nabla\eta dV = \int_\Omega \sqrt{\mathrm{detg}}e\eta dV \tag{96}$$

On the expression of tensor $\mathbf{Y}$ *(and of tensor* $\mathbf{Z}$*).* The terms figuring in the expression of the thermodynamic force $\mathbf{Z}$ in (77) read:[8]

$$\frac{\partial\|d\bar{e}\|^2_{\mathbf{g}}}{\partial\mathbf{g}^{-1}} = \frac{\partial}{\partial\mathbf{g}^{-1}}(d\bar{e}\cdot\mathbf{g}^{-1}\cdot d\bar{e}) = \frac{\partial\mathbf{g}^{-1}}{\partial\mathbf{g}^{-1}} : (d\bar{e}\otimes d\bar{e}) = \mathbb{I}^\flat{}_\# : (d\bar{e}\otimes d\bar{e}) = \mathbb{I}_\#{}^\flat : (d\bar{e}\otimes d\bar{e}) = d\bar{e}\otimes d\bar{e} \tag{99}$$

$$\frac{\partial\mathbf{g}^{-1}}{\partial\mathbf{D}} = -\mathbb{I}^\flat : \mathbb{I}_\#{}^\flat = -\mathbb{I}^\flat \tag{100}$$

The tensor $\mathbf{Z}$ can thus be written as:[9]

$$\mathbf{Z} = \frac{hc}{2}\mathbb{I}^\flat : (d\bar{e}\otimes d\bar{e}) \tag{101}$$

Finally, the expression of the dissipation rate taking into account the modified energy release rate for the 3D anisotropic ENLG model is (substituting into equation (77)):

$$\mathcal{D} = \mathbf{Y} : \dot{\mathbf{D}} = \left(\mathbf{Y}_0 + \frac{hc}{2}\mathbb{I}^\flat : (d\bar{e}\otimes d\bar{e})\right) : \dot{\mathbf{D}} \geq 0 \tag{102}$$

Since contravariant and covariant quantities are the same when the Euclidean metric is used (i.e. one has only lower indexes), the above expression can be simplified as:

$$\mathcal{D} = \left(\mathbf{Y}_0 + \frac{hc}{2}(\nabla\bar{e}\otimes\nabla\bar{e})\right) : \dot{\mathbf{D}} \geq 0 \tag{103}$$

[8]Similarly, the computation can be performed using index notation as follows:

$$\frac{\partial\|d\bar{e}\|^2_{\mathbf{g}}}{\partial\mathbf{g}^{-1}} = \frac{\partial}{\partial g^{kl}}\left(d\bar{e}_i g^{ij} d\bar{e}_j\right) = \frac{\partial g^{ij}}{\partial g^{kl}} d\bar{e}_i d\bar{e}_j = I^{ij}{}_{kl} d\bar{e}_i d\bar{e}_j = I_{kl}{}^{ij} d\bar{e}_i d\bar{e}_j = \mathbb{I}_\#{}^\flat : (d\bar{e}\otimes d\bar{e}) = d\bar{e}\otimes d\bar{e} \tag{97}$$

$$\frac{\partial\mathbf{g}^{-1}}{\partial\mathbf{D}} = \frac{\partial}{\partial D_{pq}}(q^{ij} - I^{ijkl}D_{kl}) = -I^{ijkl}\frac{\partial D_{kl}}{\partial D_{pq}} = -I^{ijkl}I_{kl}{}^{pq} = -\mathbb{I}^\flat \tag{98}$$

[9]Notice that $\mathbb{I}^\flat : (d\bar{e}\otimes d\bar{e}) \neq d\bar{e}^\flat\otimes d\bar{e}^\flat$ since the Euclidean metric is used in $\mathbb{I}^\flat$.

Damage-induced curvature of the space. For the case of the ENLG model, the Christoffel symbols are damage-dependent and read (Desmorat et al., 2015):

$$\Gamma^k_{ij} = \frac{1}{2} g^{kl} \left(g_{li,j} + g_{lj,i} - g_{ij,l} \right) = \frac{1}{2} (q_{kl} - D_{kl}) \left([(\mathbf{q} - \mathbf{D})^{-1}]_{li,j} + [\mathbf{q} - \mathbf{D})^{-1}]_{lj,i} + [(\mathbf{q} - \mathbf{D})^{-1}]_{ij,l} \right) \quad (104)$$

which induces also a damage-dependent Ricci curvature tensor (R_{ij}) by definition. A scalar measure of the curvature in the space created by damage can be obtained with the contraction $g^{ij} R_{ij}$. For an undamaged medium, the metric becomes the identity, and Christoffel symbols vanish, so the curvature is null. As pointed out by Ganghoffer (2003), further investigation is necessary to better understand the meaning of this curvature in terms of topological aspects, bridging micro-structural to a macroscopic approaches.

4.3. Isotropic ENLG model derivation

Let us now consider the isotropic ENLG damage formulation. The metric $\mathbf{g}$ is now given in local coordinates by $\mathrm{g}_{ij} = q_{ij}/(1-D)$ and its inverse $\mathbf{g}^{-1}$ reads $\mathrm{g}^{ij} = (1-D) q^{ij}$. The thermodynamic force Z in (42) can thus be written as:

$$\begin{aligned} Z &= -\frac{hc}{2} \frac{\partial \|\tilde{\nabla} \bar{e}\|^2_{\mathbf{g}}}{\partial D} \\ &= -\frac{hc}{2} \frac{\partial}{\partial D} (\mathbf{g}^{-1} \cdot d\bar{e} \cdot \mathbf{g} \cdot \mathbf{g}^{-1} \cdot d\bar{e}) \\ &= -\frac{hc}{2} \frac{\partial}{\partial D} (\mathrm{g}^{ik} d\bar{e}_k \mathrm{g}_{ij} \mathrm{g}^{jl} d\bar{e}_l) \\ &= -\frac{hc}{2} \frac{\partial}{\partial D} \left(\frac{(1-D) q^{ik} d\bar{e}_k q_{ij} (1-D) q^{jl} d\bar{e}_l}{(1-D)} \right) \\ &= \frac{hc}{2} d\bar{e}_i q^{ik} d\bar{e}_k \end{aligned} \quad (105)$$

Now, one can easily notice that $d\bar{e}_i q^{ik} d\bar{e}_k$ in (105) is a scalar product in the Euclidean space. As a consequence:

$$Z = \frac{hc}{2} \|d\bar{e}\|^2 = \frac{hc}{2} \nabla \bar{e} \cdot \nabla \bar{e} \quad (106)$$

where $\|(\cdot)\|$ is the Euclidean norm of $(\cdot)$. The expression of the dissipation rate taking into account the modified energy release rate for the full 3D isotropic ENLG model is:

$$\mathcal{D} = Y \dot{D} = \left(-3\rho \frac{\partial \psi_0}{\partial D} + \frac{hc}{2} \nabla \bar{e} \cdot \nabla \bar{e} \right) \dot{D} \geq 0 \quad (107)$$

This expression can also be obtained from the one obtained for the anisotropic model considering:

$$\mathbf{Y}_0 = -\rho \frac{\partial \psi_0}{\partial D} \mathbf{q}^{-1} \qquad \mathbf{D} = D\mathbf{q} \quad (108)$$

Replacing (108) into (102), one has:

$$\mathcal{D} = \mathbf{Y} : \dot{\mathbf{D}} = \left(-\rho \frac{\partial \psi_0}{\partial D} \mathbf{q}^{-1} + \frac{hc}{2} \mathbb{I}^{\flat} : (d\bar{e} \otimes d\bar{e}) \right) : \dot{D}\mathbf{q} = \left(-3\rho \frac{\partial \psi_0}{\partial D} + \frac{hc}{2} \nabla \bar{e} \cdot \nabla \bar{e} \right) \dot{D} = Y \dot{D} \geq 0 \quad (109)$$

4.4. Comparison with other formulations from the literature

4.4.1. Micromorphic model of Poh and Sun (2017)

A localizing gradient damage model was proposed by Poh and Sun (2017). Developed in the framework of the micromorphic theory, such a model modifies the standard thermodynamic potential proposed by Forest (2009) to account for damage-dependent non-local interactions. The free energy reads:

$$\rho\psi = \rho\psi(\boldsymbol{\epsilon}, D, \bar{e}) = \frac{1}{2}(1-D)\boldsymbol{\epsilon} : \mathbb{E} : \boldsymbol{\epsilon} + \frac{1}{2}h\left(e-\bar{e}\right)^2 + \frac{1}{2}hcg(D)\|\nabla\bar{e}\|^2 \tag{110}$$

where $g(D)$ is an exponentially decreasing function of D. It is chosen such that $g(0) = 0$ and $g(D \to 1) = R$, with $R > 0$ a small parameter accounting for residual non-local interactions.

Following usual arguments, the following Helmholtz differential equation is obtained:

$$\bar{e} - \nabla \cdot (gc\nabla\bar{e}) = e \tag{111}$$

with the boundary condition (2). Moreover, the intrinsic dissipation reads:

$$\mathcal{D} = \frac{1}{2}\left(\boldsymbol{\epsilon} : \mathbb{E} : \boldsymbol{\epsilon} - \frac{\partial g}{\partial D}hc\nabla\bar{e}\cdot\nabla\bar{e}\right)\dot{D} \geq 0 \tag{112}$$

which is always positive for $\dot{D} \geq 0$, provided that $\partial g/\partial D < 0$.

Similarities and differences. This model closely resembles the isotropic ENLG damage model, with the only difference being the decreasing function g which is introduced by the metric $\mathbf{g}$ in the ENLG model. However, this latter presents some interesting features:

(i) residual non-local interactions do not exist since the gradient term in (3) vanishes when damage approaches the unity (i.e., $\bar{e} \to e$ when $D \to 1$);

(*ii*) vanishing non-local interactions (or vanishing internal length) naturally represent damage-to-fracture transition. This means that a "pseudo-crack" can be described, and interactions between material points crossed by it are no longer allowed;

(*iii*) finally, the ENLG model does not require the introduction of additional parameters for describing the evolving interactions, as this approach relies entirely on a geometric problem description.

4.4.2. Stress-based GNL model of Vandoren and Simone (2018)

Vandoren and Simone (2018) proposed a stress-based anisotropic GNL model that builds upon the integral version introduced by Giry et al. (2011) to account for evolving internal interactions based on the stress state in the medium. The following Helmholtz differential equation was proposed:

$$\bar{e} - \nabla \cdot (\mathbf{c} \cdot \nabla\bar{e}) = e \tag{113}$$

where $\mathbf{c}$ is a second-order tensor accounting for the influence of the anisotropic stress state in the interactions. Once again, equation (113) needs to be supplemented by the Neumann boundary condition (2). Two different models can be derived, depending on the definition of tensor $\mathbf{c}$ which can be based on either the principal stress components or the equivalent stress. Additional details can be found in the cited work.

Similarities and differences. From a mathematical viewpoint, the stress-based GNL model is very similar to the ENLG one. Choosing, for instance, $\mathbf{c} = \mathbf{g}^{-1}$, the only missing term in their model is related to $\sqrt{\det \mathbf{g}} = \sqrt{\det \mathbf{c^{-1}}}$, which naturally appears in the ENLG formulation.

However, conceptually, the differences between the two formulations are more pronounced. Stress-based formulations (Giry et al., 2011; Vandoren and Simone, 2018) are suitable for modeling evolving interactions due to damage evolution and vanishing interactions close to stress-free boundaries. In contrast, the ENLG model is suitable for dealing with newly created boundaries (i.e., damaged bands) inside the considered domain only.

The influence of existing boundaries on non-local interactions is not considered in ENL formulations. However, they can be easily introduced by applying a modified metric depending on damage and stress states. For instance, one could imagine writing $\mathbf{g} = [\mathbf{c} \cdot (\mathbf{I} - \mathbf{D})]^{-1}$. A similar formulation that couples the effects of damage and stress on non-local interactions was introduced in (Negi et al., 2020). The free-energy potential proposed by the last cited paper has strong relations with the one proposed for the ENLG model based on a geometric damage description (equation (75)).

5. Numerical simulations

The isotropic ENLG and GNL damage models are implemented in a finite element toolbox developed in-house at CEA (Badri et al., 2021; Badri and Rastiello, 2023) (for testing purposes) using the FreeFEM platform. Both models are tested in the simulation of two classic problems to highlight differences and underline how the ENLG model behaves in situations where the GNL model shows some well-known drawbacks.

5.1. Damage model

An isotropic damage model with a single scalar damage variable D is considered. Following Sarkar et al. (2019) and Negi and Kumar (2022), parameter h can be taken very small compared to the Young's modulus, and the constitutive stress-strain relation is simplified as:

$$\boldsymbol{\sigma}(\boldsymbol{u}, D) = (1 - D)\mathbb{E} : \boldsymbol{\epsilon}(\boldsymbol{u}) \tag{114}$$

The damage variable ranges from zero (undamaged material) to unity (fully damaged material) according to the exponential evolution model:

$$D = 1 - \frac{\kappa_0}{\kappa}\left(1 - \alpha + \alpha e^{-B(\kappa-\kappa_0)}\right) \tag{115}$$

where:

$$\kappa = \max_t(\kappa_0, \bar{e}) \tag{116}$$

is a damage-driving history variable, $\bar{e} = \bar{e}(\boldsymbol{\varepsilon}(\boldsymbol{u}))$ is the non-local equivalent strain, κ_0 is the damage threshold, B the damage brittleness, and α is a parameter used to account for residual stresses in the behavior law. The local equivalent strain is computed according to the modified Von Mises definition (De Vree et al., 1995):

$$e = e(\boldsymbol{\varepsilon}(\boldsymbol{u})) = \frac{k-1}{2k(1-2\nu)} I_1 + \frac{1}{2k}\sqrt{\frac{(k-1)^2}{(1-2\nu)^2} I_1^2 + \frac{12k}{(1+\nu)^2} J_2'} \tag{117}$$

where ν is the Poisson's ratio, and k is a parameter corresponding to the ratio of the material strength in compression and in tension. The invariants of the strain tensor are defined as:

$$I_1 = I_1(\boldsymbol{\varepsilon}(\boldsymbol{u})) = \mathrm{Tr}(\boldsymbol{\epsilon}(\boldsymbol{u})) \tag{118}$$

$$J_2' = J_2'(\boldsymbol{\varepsilon}(\boldsymbol{u})) = \frac{1}{6}\left(3\mathrm{Tr}(\boldsymbol{\epsilon}(\boldsymbol{u}) \cdot \boldsymbol{\epsilon}(\boldsymbol{u})) - \mathrm{Tr}^2(\boldsymbol{\epsilon}(\boldsymbol{u}))\right) \tag{119}$$

5.2. Finite element implementation

The domain Ω is discretized through a finite element mesh Ω^h containing linear triangular elements (Constant Strain Triangles, CST). The unknown displacement and non-local equivalent strain fields on each finite element are approximated by linear interpolation of their nodal values.

A staggered/partitioned Picard iteration algorithm is employed to handle non-linearity (Badri et al., 2021; Badri and Rastiello, 2023). At iteration $k+1$, one first computes the $[\mathbb{P}_1, \mathbb{P}_1]$ discretized vector-valued displacement field $\boldsymbol{u}^{h,k+1} \in \mathcal{U}^h(\boldsymbol{u}^d)$ such that:

$$\int_{\Omega^h} (1 - D^{h,k})\boldsymbol{\epsilon}(\boldsymbol{u}^{h,k+1}) : \mathbb{E} : \boldsymbol{\epsilon}(\boldsymbol{v}^h)\, dV = \int_{\partial\Omega_t^h} \boldsymbol{t}^d \cdot \boldsymbol{v}^h\, dS \;\; \forall\, \boldsymbol{v}^h \in \mathcal{U}^h(\boldsymbol{0}) \tag{120}$$

and then computes the $\mathbb{P}_1$ discretized nonlocal equivalent strain field $\bar{e}^{h,k+1}$ solving:

$$\int_{\Omega^h} \frac{1}{1 - D^{h,k}}\, \bar{e}^{h,k+1}\, \eta^h dV + \int_{\Omega^h} c\nabla\bar{e}^{h,k+1} \cdot \nabla\eta^h dV = \int_{\Omega^h} \frac{1}{1 - D^{h,k}}\, e(\boldsymbol{\epsilon}(\boldsymbol{u}^{h,k+1}))\, \eta^h dV \;\; \forall \eta^h \in \mathcal{V}^h \tag{121}$$

Here, ($\mathcal{U}^h(\boldsymbol{u}^d)$, $\mathcal{U}^h(\boldsymbol{0})$, $\mathcal{V}^h$) are the discretized counterparts of ($\mathcal{U}(\boldsymbol{u}^d)$, $\mathcal{U}(\boldsymbol{0})$, $\mathcal{V}$), $D^{h,k}$ is the $\mathbb{P}_0$ discretized damage field at iteration k, and $e(\boldsymbol{\epsilon}(\boldsymbol{u}^{h,k+1}))$ is the $\mathbb{P}_0$ local strain field computed from the symetrized gradient of $\boldsymbol{u}^{h,k+1}$. At each iteration, the field $\bar{e}^{h,k+1}$ is used to update the $\mathbb{P}_0$ history variable field κ^h and compute damage. The computation is repeated till convergence at each pseudo-time step.

5.3. Four-point bending test

A notched beam is submitted to a four-point bending test (figure 3). Numerically, an increasing displacement is imposed at the loading points (denoted by the force F). The structure is discretized using three different meshes with additional refinement in the central zone of the beam. They contain 6262 (coarse mesh), 11504 (medium mesh) and 16004 (fine mesh) elements, respectively. Material parameters used in simulations are given in table 1.

Global responses. Figure 4 shows the structural responses (force vs. displacement) obtained using the ENLG and GNL models for the three considered meshes. Mesh convergence is obtained for the GNL model, whereas slight differences can be observed in the responses upon mesh refinement for the ENLG formulation. Moreover, the ENLG model gives more brittle responses than the GNL model, as is expected for evolving interaction approaches (Giry et al., 2011; Vandoren and Simone, 2018; Rastiello et al., 2018).

Damage evolution. The damage maps computed for three different imposed displacement levels using both models are depicted in figure 5. In the early phases of the test (step 1), the damage fields provided by the GNL and ENLG models are very similar (damage starts close to the notch). Then, the damaged zone computed by the GNL model becomes wider than the one obtained through the ENLG model. In this latter case, the damage field tends to localize since the early phases of the simulation (i.e., the damage tends to unity on a single line of elements) and propagates towards the upper part of the beam (step 2). At the end of the simulation (step 3), nonphysical damage spreading takes place for the GNL model around the notch. Damage is diffused in a large zone, and the expected "pseudo-crack" path cannot be described. Conversely, the damage is still localized in a smaller damage band (with $D \rightarrow 1$ on its center) about $2l_c$ in width for the ENLG model, and the nonphysical damage diffusion does not occur. Very similar behavior was described by Rastiello et al. (2018) considering an integral ENL damage model.

This feature can be even better underlined by applying a simple post-treatment of the damage field. Figure 6 shows the damage maps at the end of the simulation, considering element deletion when D exceeds the arbitrary threshold value of 0.995 at a given integration point. In the case of the GNL model, high damage levels are attained over a large region, which cannot be compared to a realistic "pseudo-crack". Conversely, the ENLG model provides a more physical "pseudo-cracking" behavior since $D \rightarrow 1$ on a single line of elements. This behavior is directly related to non-local interactions evolution during the computation. In particular, material points separated by the damage band no longer interact due to the damage-dependent Riemannian metric. Consequently, nonphysical damage spreading does not occur. The ENLG not only gives a better description of the "pseudo-crack" path compared to the GNL model but also shows promising features to naturally model damage-to-fracture transition, thus coupling CDM and Fracture Mechanics models.

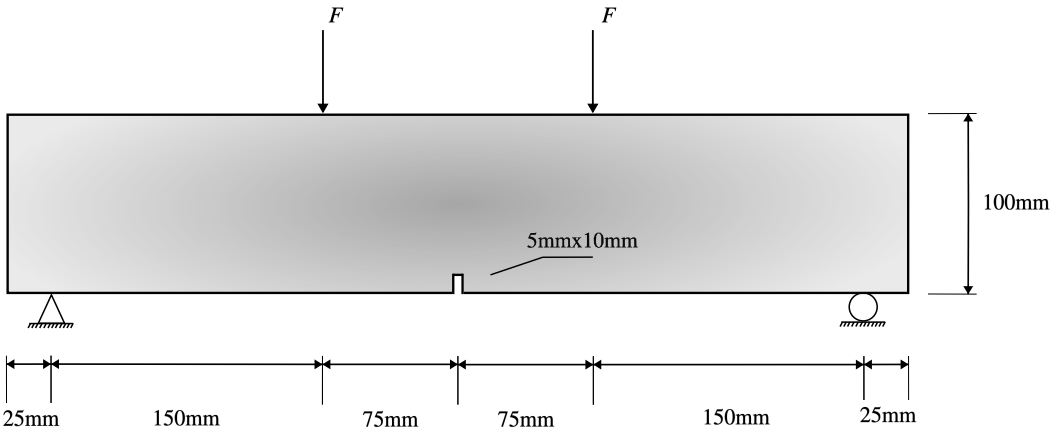

Figure 3: Four-point bending test – Geometry and boundary conditions.

5.4. Shear-band problem

The second example analyzed is the shear-band test. A square plate is submitted to a compression action on the upper boundary (figure 7). An increasing vertical displacement is applied to the top of the specimen, whereas the bottom of the specimen is constrained. Once again, three different meshes are used for the simulations. They contain 13473 (coarse mesh), 33706 (medium mesh) and 52869 elements (fine mesh), respectively. A rectangular weakened zone (with $\kappa_0^\star = \kappa_0/5$), 6x3 mm^2 in size, is placed on the bottom left of the specimen to initiate damage. Material parameters are given in table 2.

Global responses. The structural responses obtained using the GNL and ENLG models and different meshes is given in figure 8. The maximum reaction force is the same for both models. After the load peak is reached, the responses provided by the two models start to differ. Mesh convergence is obtained for the GNL model, but differences are observed in the responses provided by the ENLG model for the different meshes. A clear tendency toward mesh convergence is, however, observed.

Damage evolution. Figure 9 gives the damage maps computed using the GNL and ENLG models for three simulation steps. In the early phases of the simulation (step 1), right after the maximum reaction force, damage initiates in the weakened zone and starts to propagate diagonally in the specimen (step 2). From this point on (step 3), the size of the damage band tends to increase in the transverse direction (the band

Table 1: Four-point bending test – Material parameters.

E	c	κ_0	B	k	α	ν
[N/mm^2]	[mm^2]	[-]	[-]	[-]	[-]	[-]
40000	4	0.000075	300	10	0.92	0.2

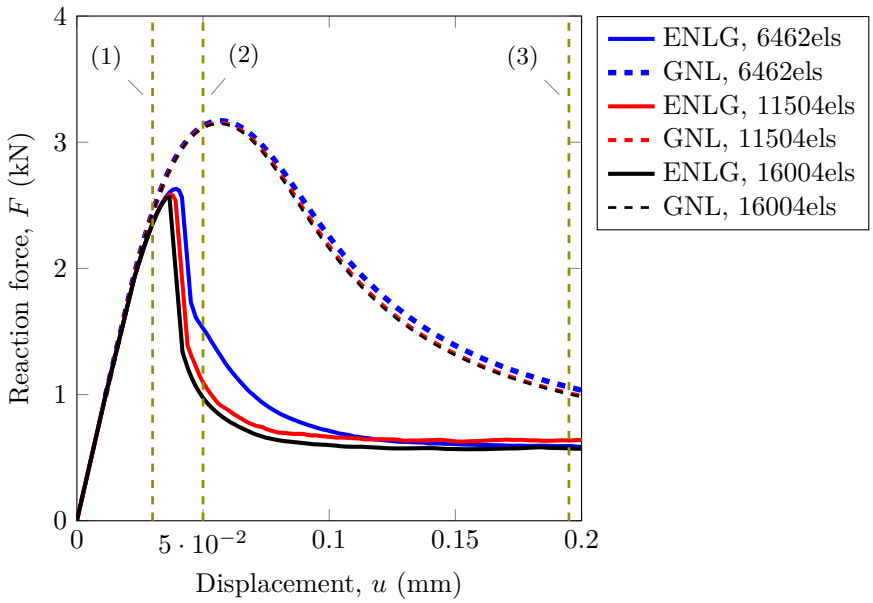

Figure 4: Four-point bending test – Structural force vs. displacement responses computed using the GNL and ENLG models and three different meshes.

enlarges). This is a well-known drawback of the classic non-local damage models. Contrarily, the shear band remains stationary for the ENLG model since no non-local interactions occur between material points. High damage levels are concentrated in a thin band a few elements width.

Such a behavior becomes clearer post-processing the results by deleting the elements where damage exceeds the threshold value of 0.999. For illustration, a very large displacement level is considered in this case ($u = 0.5$ mm). One can see that damage exceeds the threshold value in a larger zone in the case of the GNL model, whereas it tends to concentrate on almost one line of elements in the case of the ENLG model (i.e., a "pseudo-crack" is described). Once again, the ENLG model provides a more physical behavior than the GNL one.

Comments on solution oscillations. The small oscillations observed in the force vs. displacement responses illustrated in figure 8 concerning the ENLG model are related to the numerical approximation of the solution. Vandoren and Simone (2018) studied this aspect and its consequences on the damage and non-local equivalent strain evolution. They showed that, in a finite element context, the vanishing gradient parameter in (113) causes oscillations in the non-local field controlling damage evolution. In this case, mesh convergence could be affected, and minor damage spreading could take place. Such an effect is also present in the ENLG model. It is less pronounced in the 2D formulation used here since the finite element matrix related to the term c in (121) does not vanish. However, the contributions where the term $1/(1-D)$ appears can still cause this effect. Simulations in 1D and 3D of the ENLG model will inevitably show this behavior

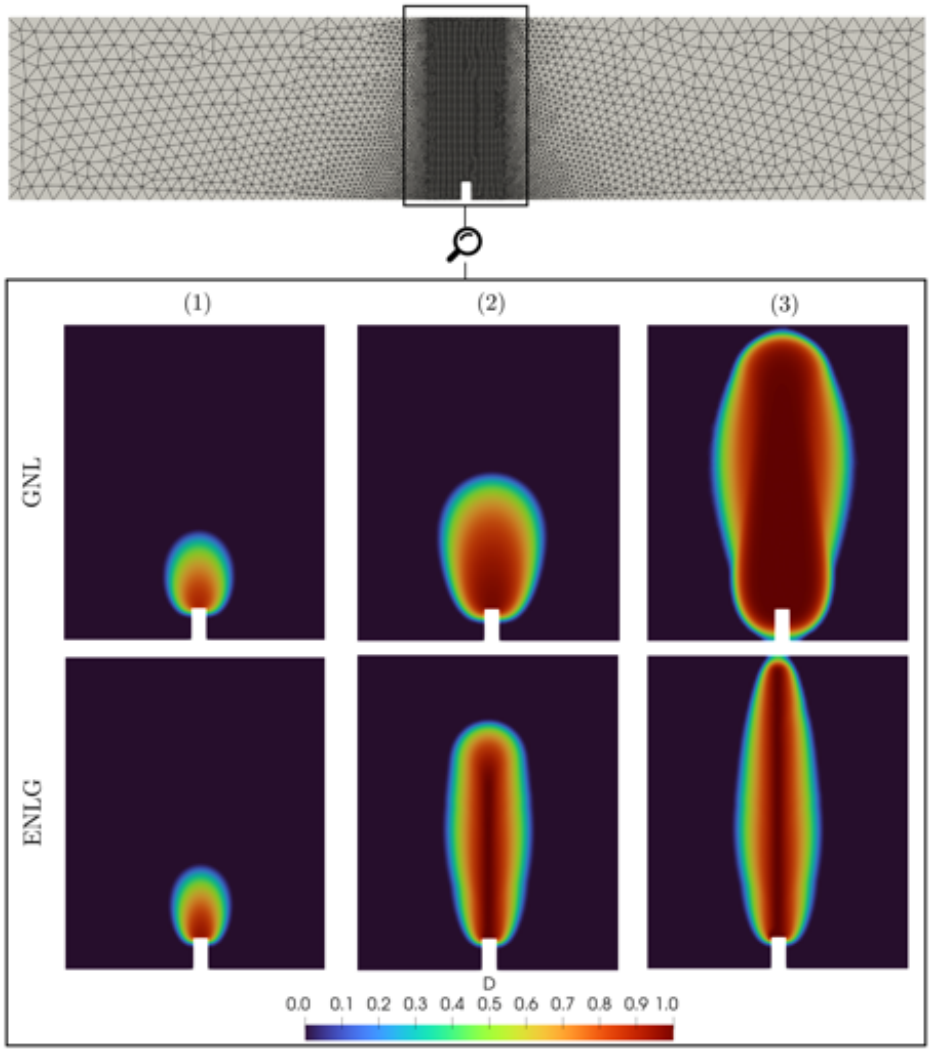

Figure 5: Four-point bending test – Damage evolution computed using the GNL and ENLG models (displacement levels identified by labels (1), (2) and (3) in figure 4).

(see Ribeiro Nogueira et al. (2022) for the 1D case) since the term related to c vanishes when $D \to 1$.

Vandoren and Simone (2018) proposed to use a minimum value of the gradient parameter to cancel non-local interactions properly and significantly reduce this effect. A similar study should be carried out for the ENLG model, which is beyond the scope of this paper. The case of the ENLG model is even more complex, as division by zero appears when $D \to 1$. However, it should be noted that from a physical viewpoint, the displacement field is no longer continuous when this condition occurs. Consequently, instead of correcting the damage formulation, strong discontinuities should be considered in the model to make it more physically and numerically robust.

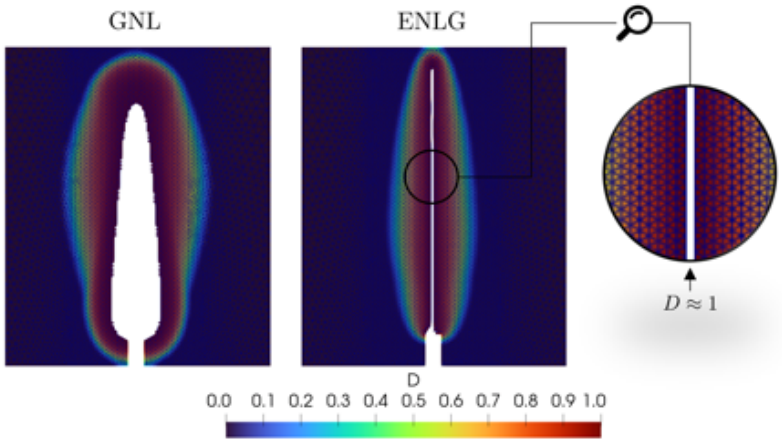

Figure 6: Four-point bending test – Damage maps at the end of the simulation (step (3) in figure 5) for the GNL and ENLG models (post-processing element deletion applied for $D > 0.995$ to identify a "pseudo-crack").

Table 2: Shear-band test – Material parameters.

E	c	κ_0	B	k	α	ν
[N/mm^2]	[mm^2]	[-]	[-]	[-]	[-]	[-]
20000	2	0.0001	100	1	0.94	0.18

6. Conclusions and perspectives

Non-local models of gradient type are often used to regularize the response of continuum damage mechanics models. Despite their capabilities in retrieving objectivity in structural response, standard approaches (e.g. the GNL model by Peerlings et al. (1996)), are incapable of describing realistic crack paths. Moreover, they often lack a proper thermodynamic framework.

This paper proposed a thermodynamic framework to derive anisotropic and isotropic ENLG damage models. Two different approaches were used, based either on a similar derivation to the one proposed for the GNL model by Peerlings et al. (2004) or inspired by the micromorphic formalism presented by Forest Forest (2009). Firstly, a straightforward modification of the free energy potential proposed for the GNL model by Peerlings et al. (2004) was proposed. It was shown that the two theories lead to similar results: the elasticity law and the energy dissipation are both modified by the evolving interactions. Considering a simplified isotropic ENLG damage formulation, it was shown, however, that the energy dissipation can become negative, which is physically unacceptable due to the non fulfillment of the Clausius-Duhem inequality. This is not due to the model assumptions but to the *ad-hoc* modification of the free energy potential by Peerlings et al. (2004) to retrieve the Helmholtz equation controlling the non-local strain evolution.

A geometric extension of the micromorphic approach was then proposed to derive the equations of the

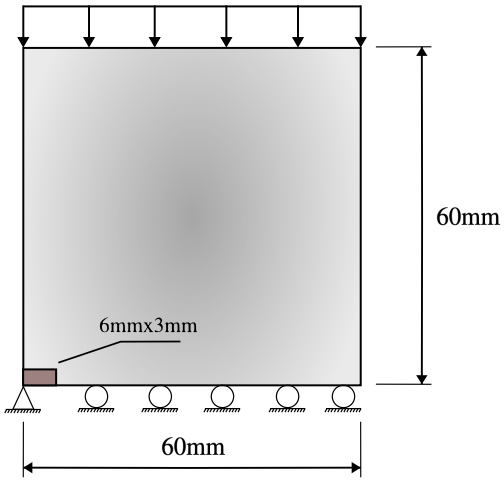

Figure 7: Shear-band test – Geometry and boundary conditions.

ENLG model. As different spaces (Euclidean and Riemannian) were considered in the original derivation of this model (Desmorat et al., 2015), it was necessary to take differential geometry considerations into account when deriving it from a thermodynamics viewpoint. Compared to the GNL model, the only modification introduced in the potential was the consideration that the non-local equivalent strain lives in a space curved by damage (Desmorat et al., 2015). Following this assumption, the original equations of the ENLG model were retrieved by applying the Laplacian-Beltrami operator, so that the term $\sqrt{\det \mathbf{g}}$ naturally appears. It was also shown that the geometric approach led to a unique expression of the energy dissipation for all the dimensions. Furthermore, it remains strictly positive, in agreement with the second principle of thermodynamics.

A simplified 2D isotropic damage variational formulation of the ENLG problem was obtained. Two numerical examples were used to highlight the advantages of considering the ENLG model instead of the GNL one. It was demonstrated that the ENLG model gives more realistic crack paths but has a more brittle behavior. In the case of the four-point bending test, the classic damage spreading around the notch, which happens for the GNL model, was not observed for the ENLG model. Moreover, the damage was concentrated in one line of elements which better describes a sort of "pseudo-crack". Similarly, the ENLG model has shown better properties when dealing with the shear-band problem. The damage band remains stationary throughout the simulation, which is not the case for the GNL model. The post-processing element deletion showed huge differences between the failure modes provided by both models, with damage localized in almost one line of elements for the ENLG model. Further investigation should be carried out to better study the numerical properties of the ENLG model, especially upon damage localization.

Further developments can be easily introduced within the framework described in this work. The exten-

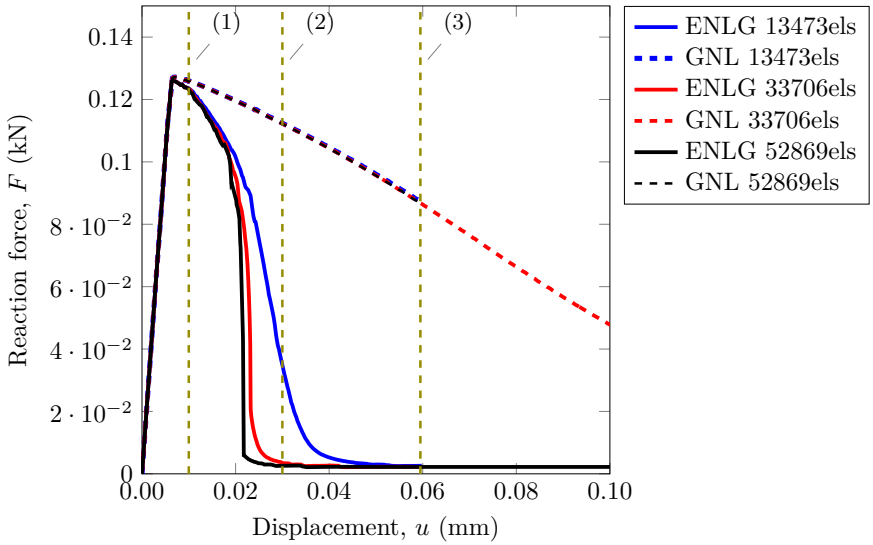

Figure 8: Shear-band test – Structural force vs. displacement responses computed using the GNL and ENLG models and three different meshes.

sion to anisotropic damage mechanics models, for instance, is straightforward. Tensorial damage behavior laws, where a second-order damage tensor is used, are suitable to be regularized with the ENLG approach since the metric is a damage-dependent second-order tensor. Another option is to consider anisotropic damage by using microplane damage models (e.g., Caner and Bažant (2013)). A classic implicit gradient regularization of these models was proposed in (Zreid and Kaliske, 2014). As the authors indicate, an extension of their method to transient evolving gradient models is necessary to have more accurate crack patterns. In both situations, the ENLG model could be helpful to describe more complex effects, such as parallel crack stress, as anisotropic internal length is naturally considered.

Finally, the transition from a regularized ENLG damage model to an explicit crack description should be considered (see, for instance, Negi and Kumar (2022)). As discussed before, the limit case where $D \to 1$ leads to a division by zero in the ENLG formulation. One has $\mathbf{g}^{-1}$ that becomes singular, given that $\det(\mathbf{g}^{-1}) \to 0$, and its inverse (the metric itself) cannot be obtained. In other words, similarly to a black hole in space-time, $D \to 1$ represents the case where a singularity appears in the space curved by damage (see figure 1). A transition to a strong discontinuity approach would be suitable not only to deal with this singularity, but also to provide direct access to crack information.

7. Acknowledgments

This work is supported by a public grant overseen by the French National research Agency (ANR) as part of the "Investissements d'Avenir" program, through the "ADI 2021" project funded by the IDEX Paris-Saclay,

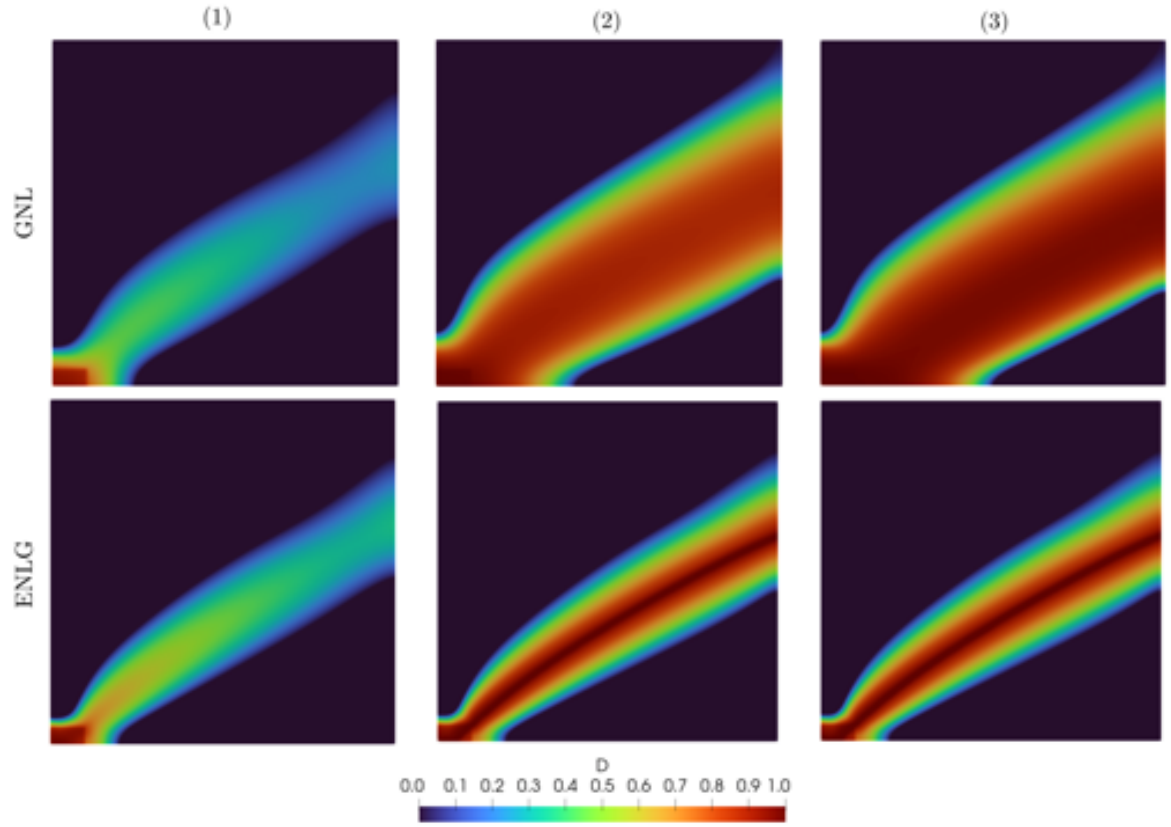

Figure 9: Shear-band test – Damage evolution computed using the GNL and ENLG models (displacement levels identified by labels (1), (2) and (3) in figure 8).

ANR-11-IDEX-0003-02. The University of Molise, Italy, is also acknowledged for its financial support.

G. Rastiello is supported by the SEISM Institute, France (https://www.institut-seism.fr/en/).

R. Desmorat, B. Kolev, and F. Loiseau (ENS Paris-Saclay) are gratefully acknowledged for exciting discussions about differential geometry in solid mechanics and their advice on the theory presented in the manuscript. B. Masseron (CEA Paris-Saclay, ENS Paris-Saclay) is also acknowledged for his advice on the manuscript.

References

Aifantis, E.C., 1984. On the microstructural origin of certain inelastic models. Journal of Engineering Materials and Technology 106, 326–330.

Badri, M.A., Rastiello, G., 2023. Hpc finite element solvers for phase-field models for fracture in solids, in: Rossi, P., Tailhan, J.L. (Eds.), Numerical Modeling Strategies for Sustainable Concrete Structures, Springer International Publishing, Cham. pp. 22–32.

Badri, M.A., Rastiello, G., Foerster, E., 2021. Preconditioning strategies for vectorial finite element linear systems arising from phase-field models for fracture mechanics. Computer Methods in Applied Mechanics and Engineering 373, 113472.

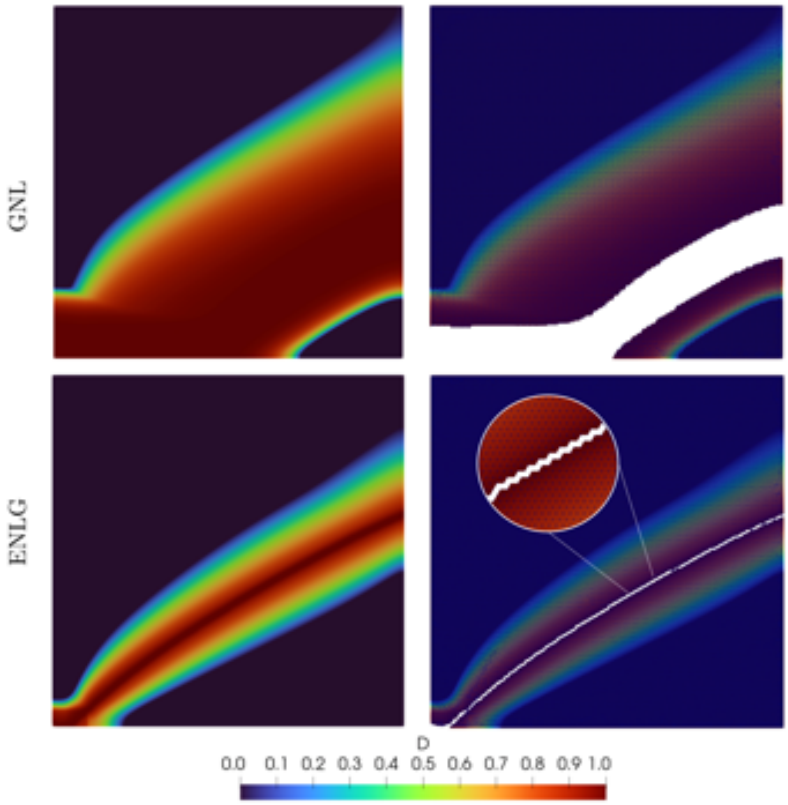

Figure 10: Shear-band test – Damage map computed for a high displacement level ($u = 0.5$ mm) (post-processing element deletion applied for $D > 0.999$ to identify a "pseudo-crack").

Bažant, Z.P., Dönmez, A.A., Nguyen, H.T., 2022. Précis of gap test results requiring reappraisal of line crack and phase-field models of fracture mechanics. Engineering Structures 250, 113285.

Benallal, A., Billardon, R., Geymonat, G., 1989. Conditions de bifurcation à l'intérieur et aux frontière pour une classe de matériaux non-standards. (bifurcation conditions inside and at the boundary for a class of non-standard materials). C. R. Acad. Sci., Paris II 308, 893–898.

Borino, G., Fuschi, P., Polizzotto, C., 1999. A Thermodynamic Approach to Nonlocal Plasticity and Related Variational Principles. Journal of Applied Mechanics 66, 952–963.

Borré, G., Maier, G., 1989. On linear versus nonlinear flow rules in strain localization analysis. Meccanica 24, 36–41. doi:10.1007/bf01576001.

Bourdin, B., Francfort, G., Marigo, J.J., 2000. Numerical experiments in revisited brittle fracture. Journal of the Mechanics and Physics of Solids 48, 797–826.

Caner, F.C., Bažant, Z.P., 2013. Microplane Model M7 for Plain Concrete. I: Formulation. Journal of Engineering Mechanics 139, 1714–1723.

Carol, I., Jirásek, M., Bažant, Z., 2001. A thermodynamically consistent approach to microplane theory. Part I. Free energy and consistent microplane stresses. International Journal of Solids and Structures 38, 2921–2931.

Chevaugeon, N., Moës, N., 2022. Lipschitz regularization for fracture: The lip-field approach. Computer Methods in Applied Mechanics and Engineering 402, 115644. A Special Issue in Honor of the Lifetime Achievements of J. Tinsley Oden.

Cosserat, E., Cosserat, F., 1909. Théorie des corps déformables. Editions Hermann, Paris.

Das, S., Sharma, S., Ramaswamy, A., Roy, D., Reddy, J.N., 2021. A Geometrically Inspired Model for Brittle Damage in Compressible Elastomers. Journal of Applied Mechanics 88, 081002.

De Vree, J., Brekelmans, W., van Gils, M., 1995. Comparison of nonlocal approaches in continuum damage mechanics. Computers & Structures 55, 581–588.

Desmorat, R., 2015. Anisotropic damage modeling of concrete materials. International Journal of Damage Mechanics 25, 818–852.

Desmorat, R., Gatuingt, F., 2007. Introduction of an internal time in nonlocal integral theories. Internal report LMT .

Desmorat, R., Gatuingt, F., Jirasek, M., 2015. Nonlocal models with damage-dependent interactions motivated by internal time. Engineering Fracture Mechanics 142, 255–275.

Desmorat, R., Gatuingt, F., Ragueneau, F., 2007. Nonlocal anisotropic damage model and related computational aspects for quasi-brittle materials. Engineering Fracture Mechanics 74, 1539–1560.

Eringen, A.C., 1999. Microcontinuum Field Theories. Springer New York, New York, NY. doi:10.1007/978-1-4612-0555-5.

Eringen, A.C., Kafadar, C.B., 1976. Polar Field Theories, in: Continuum Physics. Elsevier, pp. 1–73.

Eringen, A.C., Suhubi, E.S., 1964. Nonlinear theory of simple micro-elastic solids—I. International Journal of Engineering Science 2, 189–203.

Faria, R., Oliver, J., Cervera, M., 1998. A strain-based plastic viscous-damage model for massive concrete structures. International Journal of Solids and Structures 35, 1533–1558.

Forest, S., 2009. Micromorphic Approach for Gradient Elasticity, Viscoplasticity, and Damage. Journal of Engineering Mechanics 135, 117–131.

Francfort, G., Marigo, J.J., 1998. Revisiting brittle fracture as an energy minimization problem. Journal of the Mechanics and Physics of Solids 46, 1319–1342.

Frémond, M., Nedjar, B., 1996. Damage, gradient of damage and principle of virtual power. International Journal of Solids and Structures 33, 1083–1103.

Ganghoffer, J., 2003. New concepts in nonlocal continuum mechanics and new materials obeying a generalised continuum behaviour. International Journal of Engineering Science 41, 291–304.

Ganghoffer, J., de Borst, R., 2000. A new framework in nonlocal mechanics. International Journal of Engineering Science 38, 453–486.

Geers, M., de Borst, R., Brekelmans, W., Peerlings, R., 1998. Strain-based transient-gradient damage model for failure analyses. Computer Methods in Applied Mechanics and Engineering 160, 133–153.

Giry, C., Dufour, F., Mazars, J., 2011. Stress-based nonlocal damage model. International Journal of Solids and Structures 48(25-26), 3431–3443.

Hadamard, J., 1903. Lecons sur la Propagation des Ondes et les Équations de l'Hydrodynamique. Hermann, Paris (reedition J. Math. Phys., 11:941, 1970).

Hill, R., 1962. Acceleration waves in solids. Journal of the Mechanics and Physics of Solids 10, 1–16.

Jirásek, M., Desmorat, R., 2019. Localization analysis of nonlocal models with damage-dependent nonlocal interaction. International Journal of Solids and Structures 174-175, 1–17.

Krayani, A., Pijaudier-Cabot, G., Dufour, F., 2009. Boundary effect on weight function in nonlocal damage model. Engineering Fracture Mechanics 76, 2217–2231.

Lorentz, E., Andrieux, S., 1999. A variational formulation for nonlocal damage models. International Journal of Plasticity 15, 119–138.

Maire, J., Chaboche, J., 1997. A new formulation of continuum damage mechanics (cdm) for composite materials. Aerospace Science and Technology 1(4), 247–257.

Mandel, J., 1966. Conditions de stabilité et postulat de drucker, in: Kravtchenko, J., Sirieys, P.M. (Eds.), Rheology and Soil Mechanics / Rhéologie et Mécanique des Sols, Springer Berlin Heidelberg, Berlin, Heidelberg. pp. 58–68.

Marconi, F., 2022. Damage-fracture transition by an Eikonal-based gradient-type formulation for damage (-plastic) model. Ph.D. thesis. Université Paris-Saclay.

Mariano, P.M., 2010. Physical significance of the curvature varifold-based description of crack nucleation. Rendiconti Lincei - Matematica e Applicazioni , 215–233.

Mariano, P.M., Stazi, F.L., 2005. Computational aspects of the mechanics of complex materials. Archives of Computational Methods in Engineering 12, 391–478.

Masseron, B., Rastiello, G., Desmorat, R., 2022. Analytical strain localization analysis of isotropic and anisotropic damage models for quasi-brittle materials. International Journal of Solids and Structures , 111869.

Miehe, C., Welschinger, F., Hofacker, M., 2010. Thermodynamically consistent phase-field models of fracture: Variational principles and multi-field FE implementations. International Journal for Numerical Methods in Engineering 83, 1273–1311.

Mindlin, R.D., 1964. Micro-structure in linear elasticity. Archive for Rational Mechanics and Analysis 16, 51–78. doi:10.1007/BF00248490.

Moës, N., Chevaugeon, N., 2021. Lipschitz regularization for softening material models: the Lip-field approach. Comptes Rendus. Mécanique 349, 415–434.

Moës, N., Stolz, C., Bernard, P.E., Chevaugeon, N., 2011. A level set based model for damage growth: The thick level set approach. International Journal for Numerical Methods in Engineering 86, 358–380.

Negi, A., Kumar, S., 2022. A continuous–discontinuous localizing gradient damage framework for failure analysis of quasi-brittle materials. Computer Methods in Applied Mechanics and Engineering 390, 114434.

Negi, A., Kumar, S., Poh, L.H., 2020. A localizing gradient damage enhancement with micromorphic stress-based anisotropic nonlocal interactions. International Journal for Numerical Methods in Engineering 121, 4003–4027.

Nguyen, G.D., 2011. A damage model with evolving nonlocal interactions. International Journal of Solids and Structures 48, 1544–1559.

Peerlings, R., de Borst, R., Brekelmans, W., de Vree, J., 1996. Gradient-enhanced damage model for quasi-brittle materials. International Journal for Numerical Methods in Engineering 39, 391–403.

Peerlings, R., Massart, T., Geers, M., 2004. A thermodynamically motivated implicit gradient damage framework and its application to brick masonry cracking. Computer Methods in Applied Mechanics and Engineering 193, 3403–3417.

Pham, K., Amor, H., Marigo, J.J., Maurini, C., 2011. Gradient Damage Models and Their Use to Approximate Brittle Fracture. International Journal of Damage Mechanics 20, 618–652.

Pijaudier-Cabot, G., Haidar, K., Omar, M., Loukili, A., 2004. Non local damage models with evolving internal length: motivations and applications to coupled problems, in: Fifth International Conference on Fracture Mechanics of Concrete and Concrete Structures.

Pijaudier-Cabot, G., Bažant, Z.P., 1987. Nonlocal Damage Theory. Journal of Engineering Mechanics 113, 1512–1533.

Poh, L.H., Sun, G., 2017. Localizing gradient damage model with decreasing interactions. International Journal for Numerical Methods in Engineering 110, 503–522.

Polizzotto, C., 2003. Unified thermodynamic framework for nonlocal/gradient continuum theories. European Journal of Mechanics - A/Solids 22, 651–668.

Polizzotto, C., Borino, G., Fuschi, P., 1998. A thermodynamically consistent formulation of nonlocal and gradient plasticity. Mechanics Research Communications 25, 75–82.

Rastiello, G., Giry, C., Gatuingt, F., Desmorat, R., 2018. From diffuse damage to strain localization from an eikonal non-local (enl) continuum damage model with evolving internal length. Computer Methods in Applied Mechanics and Engineering 113, 1512–1233.

Ribeiro Nogueira, B., Giry, C., Rastiello, G., Gatuingt, F., 2022. One-dimensional study of boundary effects and damage diffusion for regularized damage models. Comptes Rendus. Mécanique 350, 507–546.

Richard, B., Ragueneau, F., Cremonac, C., Adelaide, L., 2010. Isotropic continuum damage mechanics for concrete under cyclic loading: Stiffness recovery, inelastic strains and frictional sliding. Engineering Fracture Mechanics 77, 1203–1223.

Rudnicki, J., Rice, J., 1975. Conditions for the localization of deformation in pressure-sensitive dilatant materials. Journal of the

Mechanics and Physics of Solids 23, 371–394.

Sarkar, S., Singh, I., Mishra, B., Shedbale, A., Poh, L., 2019. A comparative study and ABAQUS implementation of conventional and localizing gradient enhanced damage models. Finite Elements in Analysis and Design 160, 1–31.

Saroukhani, S., Vafadari, R., Simone, A., 2013. A simplified implementation of a gradient-enhanced damage model with transient length scale effects. Computational Mechanics 51, 899–909.

Simone, A., Askes, H., Sluys, L.J., 2004. Incorrect initiation and propagation of failure in non-local and gradient-enhanced media. International Journal of Solids and Structures 41, 351–363.

Simone, A., Wells, G.N., Sluys, L.J., 2003. From continuous to discontinuous failure in a gradient-enhanced continuum damage model. Computer Methods in Applied Mechanics and Engineering 192, 4581–4607.

Steinmann, P., Carol, I., 1998. A framework for geometrically nonlinear continuum damage mechanics. International Journal of Engineering Science 36, 1793–1814.

Suhubl, E.S., Eringen, A.C., 1964. Nonlinear theory of micro-elastic solids—II. International Journal of Engineering Science 2, 389–404.

The Sage Developers, 2022. SageMath, the Sage Mathematics Software System (Version 9.7). `https://www.sagemath.org`.

Thierry, F., Rastiello, G., Giry, C., Gatuingt, F., 2020. One-dimensional eikonal non-local (enl) damage models: Influence of the integration rule for computing interaction distances and indirect loading control on damage localization. Mechanics Research Communications 110, 103620.

Thomas, T., 1961. Plastic Flow and Fracture in Solids by Tracy Y Thomas. ISSN, Elsevier Science.

Vandoren, B., Simone, A., 2018. Modeling and simulation of quasi-brittle failure with continuous anisotropic stress-based gradient-enhanced damage models. Computer Methods in Applied Mechanics and Engineering 332, 644–685.

Zafati, E., Richard, B., 2019. Anisotropic continuum damage constitutive model to describe the cyclic response of quasi-brittle materials: The regularized unilateral effect. International Journal of Solids and Structures 162, 164–180.

Zreid, I., Kaliske, M., 2014. Regularization of microplane damage models using an implicit gradient enhancement. International Journal of Solids and Structures 51, 3480–3489.